© 2020. Published by The Company of Biologists Ltd | Journal of Cell Science (2020) 133, jcs242404. doi:10.1242/jcs.242404

RESEARCH ARTICLE

# Induction of ligand promiscuity of αVβ3 integrin by mechanical force

**Michael Bachmann[1,2,*], Markus Schäfer[1,3,*], Vasyl V. Mykuliak[4], Marta Ripamonti[2], Lia Heiser[1], Kai Weißenbruch[1], Sarah Krübel[1], Clemens M. Franz[5,6], Vesa P. Hytönen[4], Bernhard Wehrle-Haller[2,‡] and Martin Bastmeyer[1,3,‡]**

## ABSTRACT

αVβ3 integrin can bind to multiple extracellular matrix proteins, including vitronectin (Vn) and fibronectin (Fn), which are often presented to cells in culture as homogenous substrates. However, in tissues, cells experience highly complex and changing environments. To better understand integrin ligand selection in such complex environments, we employed binary-choice substrates of Fn and Vn to dissect αVβ3 integrin-mediated binding to different ligands on the subcellular scale. Super-resolution imaging revealed that αVβ3 integrin preferred binding to Vn under various conditions. In contrast, binding to Fn required higher mechanical load on αVβ3 integrin. Integrin mutations, structural analysis and chemical inhibition experiments indicated that the degree of hybrid domain swing-out is relevant for the selection between Fn and Vn; only a force-mediated, full hybrid domain swing-out facilitated αVβ3-Fn binding. Thus, force-dependent conformational changes in αVβ3 integrin increased the diversity of available ligands for binding and therefore enhanced the ligand promiscuity of this integrin.

This article has an associated First Person interview with the first author of the paper.

**KEY WORDS: αVβ3 integrin, ECM, Ligand selection, Focal adhesions, Fibronectin, Mechanosensing**

## INTRODUCTION

Integrins are important cell adhesion receptors and consist of α- and β-subunits forming transmembrane heterodimers (Bachmann et al., 2019; Campbell and Humphries, 2011). In their active state, the extracellular part binds to proteins of the extracellular matrix (ECM) or proteins on other cells, while the intracellular part is connected to actin via multiple adapter and signaling proteins that make up the so-called adhesome (Byron et al., 2011; Hytönen and Wehrle-Haller, 2014; Kuo et al., 2011; Schiller et al., 2013). Activating integrins requires conformational changes that include extension of the extracellular domains and opening of the integrin headpiece. The respective steps in activation are named bent-closed, extended-closed and finally extended-open conformation. In β-integrin subunits, headpiece opening is characterized by the swing-out of the hybrid domain from the βI-like domain (Eng et al., 2011; Zhu and Springer, 2013). Molecular dynamics (MD) simulations indicated that force supports this hybrid domain swing-out and thereby leads to full integrin activation (Puklin-Faucher et al., 2006; Zhu et al., 2008). The best-studied cases of force-dependent ligand-integrin interactions are the binding of αVβ3 and α5β1 integrin to fibronectin (Fn) (Engler et al., 2009; Fernandez-Sauze et al., 2009; Takahashi et al., 2007; van der Flier et al., 2010). Considerable effort has been invested to understand individual and cooperative effects of this αVβ3/Fn and α5β1/Fn binding (Benito-Jardón et al., 2017; Roca-Cusachs et al., 2009; Schiller et al., 2013; White et al., 2007). At the same time, however, it is less clear how an individual integrin can discriminate between different ligands. Work with the RGD peptide (ligand binding site for αVβ3 and α5β1, among several other integrins) has indicated that conformational changes around the RGD sequence (cyclic versus linear peptide) can cause integrin selectivity (Mas-Moruno et al., 2010; Pierschbacher and Ruoslahti, 1987). But whether these findings have a relevance for physiological ligands remained to be tested. At the same time, more than 12 potential RGD ligands for αVβ3 integrin have been reported (Humphries et al., 2006), but it remains unclear whether or how these ligands are selected by αVβ3 integrin. We have recently developed a method to produce microstructured Fn/vitronectin (Vn) substrates to analyze ligand selection by αVβ3 integrin on a cellular level (Pinon et al., 2014; Rahikainen et al., 2017; Soto-Ribeiro et al., 2019). Fn is a structural component of the ECM and has essential functions during development (George et al., 1993). Vn is a matrisomal protein with no relevant structural role for the ECM, while regulating inflammation and wound healing in healthy and in cancer settings (Gladson et al., 1995; Keasey et al., 2018; Preissner and Reuning, 2011). Interestingly, both Fn and Vn are present at high concentrations in the blood [Fn, 300 µg/ml (Pankov and Yamada, 2002); Vn, 200–400 µg/ml (Preissner and Reuning, 2011)], suggesting a need for fibroblasts to select between these different ECM proteins after wounding.

Here, we combined Fn/Vn substrates with super-resolution microscopy and super-resolution live-cell imaging. We analyzed the interaction of αVβ3 integrin with different ligands by using αVβ3 integrin mutants and pharmacological inhibitors. We found a clear preference of αVβ3 integrin for Vn under a wide range of conditions. Surprisingly, we revealed that mechanical load on αVβ3 integrin enabled Fn binding, while Vn is already recognized by

[1]Zoological Institute, Cell and Neurobiology, Karlsruhe Institute of Technology (KIT), Karlsruhe 76131, Germany. [2]Department of Cell Physiology and Metabolism, University of Geneva, Geneva 1211, Switzerland. [3]Institute of Functional Interfaces (IFG), Karlsruhe Institute of Technology (KIT), Eggenstein-Leopoldshafen 76344, Germany. [4]Faculty of Medicine and Health Technology and BioMediTech, Tampere University, and Fimlab Laboratories, Tampere 33014, Finland. [5]DFG–Center for Functional Nanostructures, Karlsruhe Institute of Technology (KIT), Karlsruhe 76131, Germany. [6]WPI Nano Life Science Institute, Kanazawa University, Kanazawa 920-1192, Japan.
*These authors contributed equally to this work

‡Authors for correspondence (bernhard.wehrle-haller@unige.ch; martin.bastmeyer@kit.edu)

M.Bachmann, 0000-0001-9450-3458; M.S., 0000-0002-1297-3745; V.V.M., 0000-0002-2522-9907; L.H., 0000-0002-0849-6501; C.M.F., 0000-0003-0104-4841; V.P.H., 0000-0002-9357-1480; B.W., 0000-0002-1159-1147

**Handling Editor: Arnoud Sonnenberg**
**Received 3 December 2019; Accepted 12 March 2020**

Journal of Cell Science (2020) 133, jcs242404. doi:10.1242/jcs.242404

αVβ3 integrin under lower mechanical load. Additional experiments indicated that this selection of ligands is coupled to force-regulated integrin conformations. Under low-force conditions, or when mutationally prevented from full headpiece opening, αVβ3 integrin binds only to Vn. However, mechanical pull induces a full hybrid domain swing-out to the extended-open conformation (Puklin-Faucher et al., 2006; Zhu et al., 2008). In this conformation, αVβ3 integrin gains the ability to bind to Fn, indicating a more promiscuous integrin-ligand relationship. We further show that these ligand-binding properties modulate cellular behavior during spreading, migration and mechanotransduction, depending on the respective ECM protein. Finally, we established additional ligand combinations and found that osteopontin (Opn) phenocopied Vn in binary-choice substrates, while fibrinogen (Fbg) resembled Fn. This indicates that the mechanism of differential ligand selectivity of αVβ3 integrin can be transferred to a wider range of integrin-ligand combinations.

## RESULTS

### Vn is the preferred ligand for αVβ3 integrin

To study how the simultaneous presentation of two ECM ligands influences the binding choice of αVβ3 integrin, we produced Fn/Vn substrates with subcellular resolution (Pinon et al., 2014). To do this, 2×2 µm squares of Fn separated by 1 µm gaps were stamped onto a coverslip and the remaining surface was covered with Vn, leading to a clear separation of both proteins with a geometrical coverage of equal contribution (Pinon et al., 2014). The quality of substrates was analyzed by fluorescence and atomic force microscopy (AFM) (Fig. 1A,B). To specifically analyze GFP-tagged β3 integrin without competition by endogenous αVβ3 integrin, we used a subclone of NIH3T3 cells expressing low levels of endogenous β3 integrin (Fig. S1A; Pinon et al., 2014). Furthermore, in these cells, αV integrin is the only subunit pairing with β3 integrin. Thus, our results with β3 integrin are synonymous for αVβ3 integrin. To study the binding choice of αVβ3 integrin on Fn/Vn substrates, cells were transfected with GFP-tagged β3-wild-type (wt) integrin, cultured for 2 h and immunolabeled. Paxillin was used as a marker to detect all integrin-mediated adhesions. Super-resolution structured illumination microscopy (SR-SIM) revealed paxillin clusters on both Fn- and Vn-coated areas. In contrast, αVβ3 integrin revealed a strong preference to Vn (83.5% colocalization; Fig. 1C,D). This preference was not dependent on the size of αVβ3 integrin-mediated adhesions (Fig. 1F). To exclude that the low amount of αVβ3 integrin on Fn is caused by competition and steric hindrance with endogenous α5β1 integrin, we tested β1 integrin-deficient GD25 cells on Fn/Vn substrates. We observed the same preference of αVβ3 integrin for Vn (82.8%; Fig. S1D,F). Furthermore, this preference for Vn was reproducible for a wide range of experimental conditions, such as pattern geometry and stamping order (Fig. S1G,I), the ratio of Fn/Vn used to prepare Fn/Vn substrates (Fig. S1B) or substrate stiffness (Fig. S1J–L). Substrates homogenously coated with either Fn or Vn also supported these findings: Both area and intensity of αVβ3 integrin adhesions are significantly increased on Vn compared to Fn (Fig. S2).

Next, we measured the interaction of αVβ3 integrin with Fn and Vn *in vitro* using biolayer interferometry (Fig. 1E). Whereas Fn dissociated rapidly from αVβ3 integrin, Vn binding to αVβ3 was non-dissociable. Work by Orlando and Cheresh also observed non-dissociable binding between Vn and αVβ3 (Orlando and Cheresh, 1991), contrasting with work by Chillakuri and colleagues (Chillakuri et al., 2010). To test our findings in light of these contradicting observations, we analyzed Vn-αVβ3 integrin interaction in the presence of the RGD mimetic αVβ3 integrin inhibitor cilengitide (Fig. S3E). The dissociation of Vn from αVβ3 integrin in the presence of cilengitide confirmed that we observed a specific, RGD-dependent interaction between Vn and αVβ3 integrin (Fig. 1E). This corroborates our finding of a non-dissociable, RGD-dependent interaction between αVβ3 integrin and Vn in this *in vitro* assay. However, such a difference in binding behavior might also imply that αVβ3 integrin binding to Fn is unlikely whenever Vn is present. In contrast, on Fn/Vn substrates, we observed a colocalization of αVβ3 integrin with Fn of 16.5% (Fig. 1C,D). To understand the binding of αVβ3 integrin to Fn in a cellular context, we studied the dynamics of αVβ3 integrin-mediated adhesion formation in living cells. First, we performed AFM-based single-cell force spectroscopy (Dao et al., 2012; Langhe et al., 2016). β1-deficient GD25 cells were attached to the AFM cantilever and alternatingly brought into contact with homogenously coated Fn and Vn areas. Detachment forces during cell retraction were measured after 10 s, 30 s and 120 s of contact. After 30 s and 120 s of adhesion, significantly higher forces were needed to detach cells from Vn compared to Fn (Fig. 1G), indicating that αVβ3 integrin-mediated adhesions formed and/or matured faster on Vn. Next, we observed β3-wt GFP-expressing NIH3T3 cells on Fn/Vn substrates using SR-SIM live-cell imaging. During spreading, cells initiated numerous nascent adhesions on these binary-choice substrates (Fig. 1H; Movies 1 and 2). These αVβ3 integrin-mediated adhesions almost exclusively formed on Vn (Fig. 1I), while during adhesion maturation, some adhesions were translocated onto Fn in a centripetal direction towards the cell center and in the direction of retrograde actin flow (yellow arrows in Fig. 1H; Movie 2). Thus, observed *in vitro* and in a cellular context, αVβ3 integrin prefers binding to Vn over Fn. Interestingly, live-cell imaging indicated that actin flow – and therefore mechanical forces – might be an important parameter involved in the binding of Fn by αVβ3 integrin.

### Actomyosin contractility regulates the ligand preference of αVβ3 integrin

To test whether intracellular forces are involved in the binding choice of αVβ3 integrin, we reduced actomyosin contractility with blebbistatin or Y27632. Blebbistatin inhibits myosin directly, while Y27632 inhibits the Rho/ROCK pathway and thereby reduces myosin activity. Both inhibitors increased the number of small, round nascent adhesions in the cell periphery (Fig. 2A,B) and additionally caused a significant decrease in colocalization of β3-wt GFP integrin with Fn (Fig. 2G; Fig. S3A; ≈2.5-fold decrease). Incubating cells for 6 h in the presence of blebbistatin caused no improvement in Fn localization of αVβ3 integrin, indicating that reduced contractility does not delay but rather prevents Fn binding by αVβ3 integrin (Fig. S1C,H). Vinculin is well established as an important part of the molecular clutch to transmit forces from actin to the integrin-ECM bond (Humphries et al., 2007; Rahikainen et al., 2017; Thievessen et al., 2013). Therefore, we analyzed the localization of β3-wt GFP integrin on Fn/Vn substrates in mouse embryonic fibroblasts (MEFs) derived from vinculin knockout mice (MEF Vcl$^{-/-}$). Indeed, the absence of vinculin caused a decrease in Fn binding of αVβ3 GFP integrin (Fig. 2E,H), which was comparable to that after blebbistatin or Y27632 treatment (Fig. 2G). In contrast, re-expression of vinculin mCherry in MEF Vcl$^{-/-}$ increased the Fn localization of αVβ3 GFP integrin to control levels (Fig. 2D,F,H). To enhance the mechanical load on integrins, we overexpressed non-muscle myosin IIA mApple (NMIIA) in NIH3T3 cells (Fig. 2C). Additional NMIIA caused an increase in αVβ3 GFP integrin localization on Fn (Fig. 2G;

Journal of Cell Science (2020) 133, jcs242404. doi:10.1242/jcs.242404

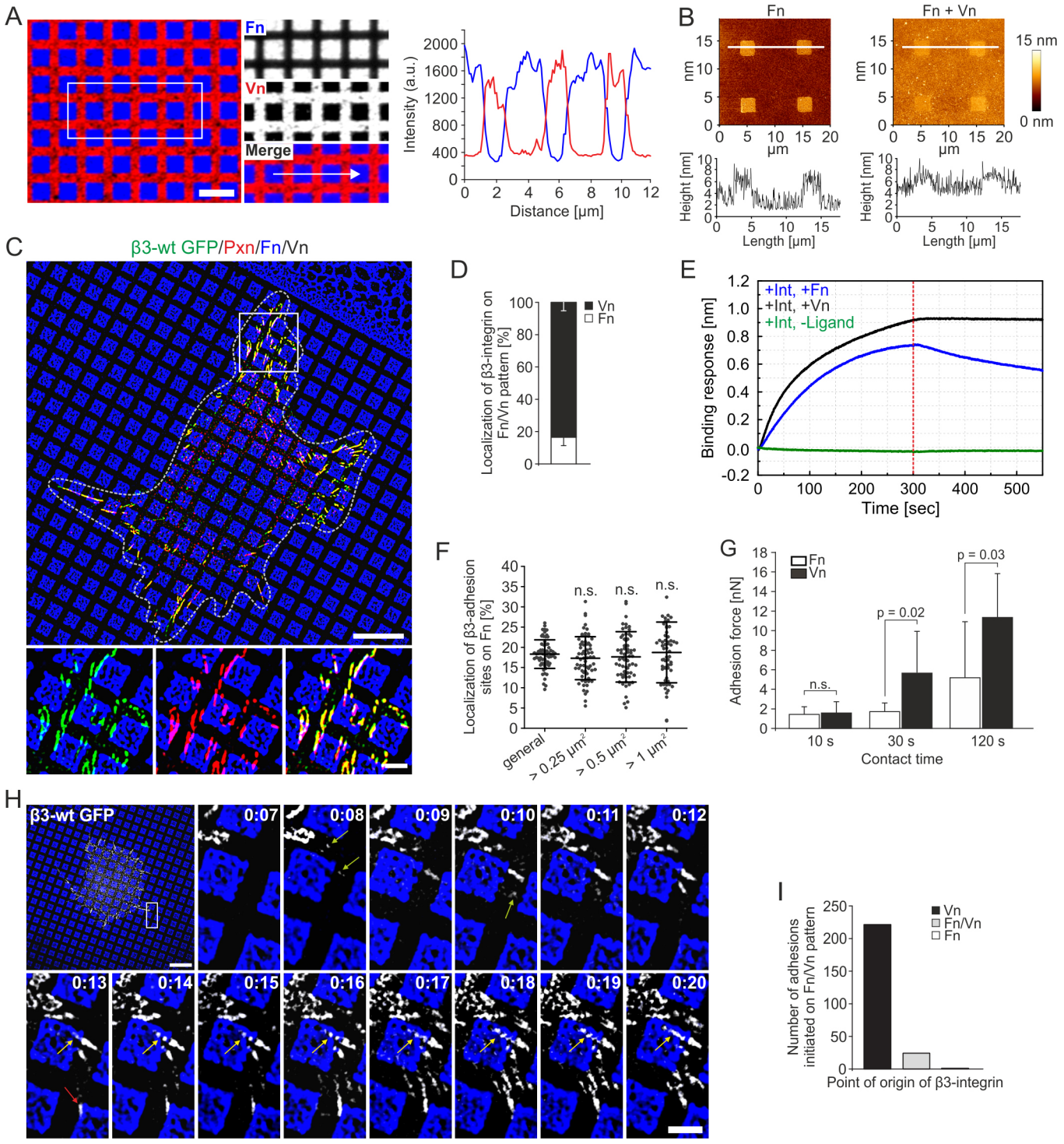


**Fig. 1.** See next page for legend.

≈1.5-fold increase). Taken together, these findings indicate that αVβ3 integrin binding to Fn is fostered by intracellular force and vinculin, whereas Vn is recognized by αVβ3 integrins already under low mechanical load.

### Hybrid domain swing-out is required for Fn binding of αVβ3 integrin

Next, we asked whether enhanced activation of αVβ3 integrin could substitute mechanical forces during Fn binding. Therefore, we employed either $Mn^{2+}$ activation of αVβ3 integrin (Fig. 3A) or established mutations to activate integrins (Fig. 3B–D): (1) $Mn^{2+}$ treatment increases the affinity of the integrin headpiece for the ligand (Zhu and Springer, 2013); (2) the β3-VE mutation has a 20-fold higher affinity for talin than for talin than β3-wt (Pinon et al., 2014); (3) the β3-D723A mutation disrupts the inhibitory salt bridge at the inner membrane clasp between the αV and β3 subunits (Saltel et al., 2009); and (4) β3-N305T has been reported to cause a constitutive hybrid domain swing-out and slower integrin dynamics

Journal of Cell Science (2020) 133, jcs242404. doi:10.1242/jcs.242404

**Fig. 1. αVβ3 integrin favors binding to vitronectin (Vn) compared to fibronectin (Fn).** (A) Microcontact printing of 2×2 µm squares of Alexa Fluor 647-labeled Fn (blue) onto glass cover slips and backfilling the pattern with Alexa Fluor 568-labeled Vn (red) leads to differential Fn/Vn patterns (profile along the arrow). Geometrical coverage varies slightly: 44–49% Fn, 56–51% Vn. a.u., arbitrary units. (B) Height profiles of Fn patterns (left) and Fn/Vn patterns (right) measured with atomic force microscopy (AFM) in contact mode. Profiles along the white lines indicate a monolayer of Fn and a uniform topography of the binary-choice substrates. (C) Super-resolution structured illumination microscopy (SR-SIM) image of NIH3T3 cell transfected with β3-wt GFP integrin (green), cultured on Fn/Vn pattern (Fn blue) and immunostained for paxillin (red). Cell contour is outlined with a dashed white line. (D) Quantification of colocalization of β3-wt GFP integrin with Fn or Vn for fixed cells ($n$=66; $N$=4). (E) Representative curves for Fn and Vn association (0 s to 300 s) and dissociation (300 s to 550 s) to αVβ3 integrin measured *in vitro* with biolayer interferometry. (F) Quantification of colocalization of β3-wt GFP integrin with Fn for all adhesions ('general') or only for those bigger than the indicated threshold (re-analysis of the data from D). n.s., not significant. (G) Single-cell force spectroscopy of GD25 cells (expressing αVβ3, but no β1 integrin). Detachment forces on Fn and Vn measured after the indicated contact time points. Typically, ten force measurement repetitions were performed for each cell and time point, and a total of eight cells were tested. (H) NIH3T3 cell transfected with β3-wt GFP integrin (white) seeded on Fn/Vn patterns (Fn blue) was monitored with live-cell SR-SIM (Movie 1). Magnifications show initiation and maturation of αVβ3-mediated adhesions (time in h:min). Green arrows point to newly established adhesions. Yellow arrows follow adhesions that initiated on Vn while they translocate to Fn. The red arrow at 13 min indicates an adhesion that appeared at the Fn/Vn interface. (I) Total number of αVβ3-mediated adhesions that initiated on Vn or Fn, or at the Fn/Vn interface for cells imaged with live-cell SR-SIM. Quantification is based on 246 initiated adhesions from six cells out of three independent experiments. Scale bars: 10 µm in overviews, 2 µm in zoom-ins (C,H); 5 µm (A).

(Cluzel et al., 2005; Luo et al., 2003). Surprisingly, on Fn/Vn substrates, only β3-N305T showed a significant increase in colocalization with Fn (Fig. 3F; ≈1.5-fold increase), whereas $Mn^{2+}$ treatment and the intracellular activating mutations (β3-VE and β3-D723A) caused no significant difference. However, Vn remained the preferred ligand for all conditions. Importantly, endogenous αVβ3 integrin is basically absent in the NIH3T3 cells we used (Fig. S1A) and therefore does not compete with β3 mutations used in this experiment. Next, we used SR-SIM live-cell imaging to test whether the conformational changes caused by the β3-N305T mutation are accompanied by the ability to initiate adhesions on Fn (Fig. 3J; Movies 3 and 4). We observed that spreading cells initiated most β3-N305T-mediated adhesions on Vn but, in contrast to β3-wt integrin, few adhesions initiated on Fn as well (Fig. 3K). The mutation β3-VE caused a non-significant but observable increase in Fn colocalization (Fig. 3F). However, β3-VE failed to initiate adhesions on Fn similar to β3-wt (Fig. 3K; Movies 5 and 6), again highlighting the relevance of the headpiece opening, rather than talin-mediated β3 integrin activation, for Fn binding.

Interestingly, all activating conditions caused central clusters of αVβ3 integrin with irregular shapes compared to peripheral adhesions (Fig. 3A–D, zoom-in 2). Similar integrin clusters have been reported to appear within minutes after $Mn^{2+}$ addition (Cluzel et al., 2005; Saltel et al., 2009). On Fn/Vn substrates, these clusters were almost exclusively localized on Vn (Fig. S3F). Analysis of several integrin adapter proteins demonstrated talin recruitment but no association of paxillin, vinculin or actin stress fibers to these αVβ3 integrin clusters (Fig. 3A–D; Fig. S3G–I). This suggests that they are not mechanically coupled to the actin cytoskeleton and thus are under low mechanical load (compare to MEF $Vcl^{-/-}$; Fig. 2E,H). The exclusive localization of these 'low-force adhesions' on Vn confirms our observations using contractility inhibitors and MEF Vcl $^{-/-}$ and emphasizes the requirement of mechanical load on αVβ3 integrin to bind to Fn, in contrast to Vn.

In summary, our experiments showed that only αVβ3 integrin activation by the N305T mutation increases Fn localization of αVβ3-mediated focal adhesions. Furthermore, β3-N305T allows the initiation of adhesions on Fn in contrast to other β3 integrin-activating conditions. This indicates that hybrid domain swing-out is a crucial step for the ability of αVβ3 integrin to bind to Fn.

## Complete force-dependent hybrid domain swing-out is necessary for Fn binding

The unique ability of β3-N305T to increase Fn binding (Fig. 3F) motivated us to study this mutation in more detail. The creation of a glycosylation site between the βI-like and the hybrid domain at Asn 303 (N303) is proposed to cause a constitutive hybrid domain swing-out and thereby full integrin activation. To experimentally dissect the steric effect of N303 glycosylation from force-induced hybrid domain swing-out (Puklin-Faucher et al., 2006; Zhu et al., 2008), we treated β3-N305T-expressing cells with blebbistatin (Fig. 3E). β3-N305T-mediated adhesions appeared less affected by blebbistatin compared to β3-wt (compare to Fig. 2A; 10 µM blebbistatin in both experiments). Whereas β3-wt only formed nascent adhesions, β3-N305T showed both nascent adhesions and partially matured, elongated adhesions. However, the colocalization of β3-N305T GFP with Fn was clearly reduced in the case of reduced cellular contractility (Fig. 3G; ≈5-fold decrease). This indicates that the conformational change induced by the glycan wedge alone may not be sufficient to increase Fn binding in the absence of mechanical forces on αVβ3 integrin. We observed the same effect of reduced Fn binding for all other activating conditions when combined with blebbistatin treatment (Fig. S3B). Thus, all integrin-activating conditions relied on mechanical forces for Fn binding of αVβ3 integrin. Even constitutive hybrid domain swing-out as reported for the β3-N305T mutation was not sufficient for efficient Fn binding in conditions of reduced cellular contractility. Apparently, mechanical forces caused additional conformational changes needed for Fn binding.

To understand the impact of force and glycosylation on αVβ3 integrin conformation, we employed MD simulations for a αVβ3 integrin structure that was glycosylated at N303. Zhu and colleagues published headpiece opening of αIIbβ3 integrin in eight steps (Zhu and Springer, 2013). We used an Fn-bound structure of αVβ3 integrin [RCSB Protein Data Bank (PDB): 4MMX] and arranged a hybrid domain swing-out by superimposition with step 7 (PDB: 3ZE1; chain B) in the activation cascade of αIIbβ3 described by Zhu and colleagues. This structure was modified by adding a glycosylation at N303 and equilibrating for 100 ns. The same structure without glycosylation at N303 was used as a control. MD simulations showed that hybrid domains swung out to a similar angle, while the glycosylated form appeared more stable (Fig. 3H,I). Accordingly, glycosylation at N303 might stabilize αVβ3 integrin in a conformation close to full activation. However, the final activation step [step 8 (Zhu and Springer, 2013); PBD: 3ZE2, chain C, D], is characterized by an even further increase in the hybrid domain swing-out ('Fully activated 1' in Fig. 3L). Another published structure of the fully open β3 integrin headpiece (PBD: 3FCU, αIIbβ3) showed a similar maximal hybrid domain swing-out ('Fully activated 2' in Fig. 3L). Thus, comparison of glycosylated and fully activated structures suggested that N303 glycosylation alone is not sufficient to induce the full hybrid domain swing-out. Combining β3-N305T with $Mn^{2+}$ showed no additive effect on Fn binding (Fig. 3G), as was the case for adding $Mn^{2+}$ to β3-wt (Fig. 3F).

Journal of Cell Science (2020) 133, jcs242404. doi:10.1242/jcs.242404

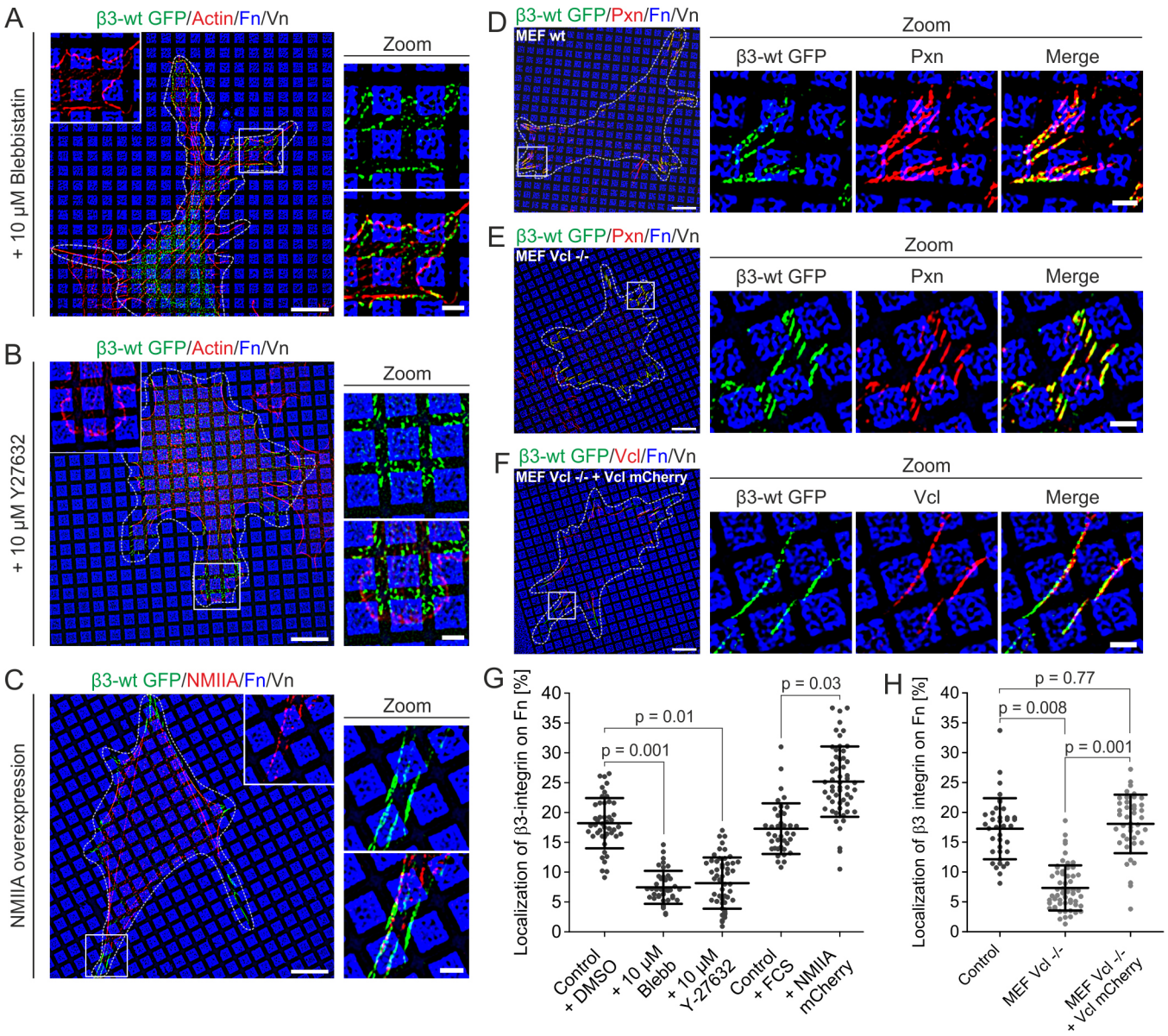


**Fig. 2. Cell contractility regulates ligand preference of αVβ3 integrin.** (A) NIH3T3 cells transfected with β3-wt GFP integrin (green) were cultured on Fn/Vn substrates (Fn in blue) in the presence of 10 μM blebbistatin and were stained after fixation for actin (red). (B) NIH3T3 cells treated with 10 μM Y27632. (C) NIH3T3 cells transfected with β3-wt GFP integrin (green) and myosin IIA mApple (NMIIA; red) with serum (FCS; 10%) present in the medium. (D,E) MEF wt (D) or MEF vinculin knockout cells (MEF Vcl$^{-/-}$) (E) transfected with β3-wt GFP integrin (green) and immunostained for paxillin (Pxn; red). (F) MEF Vcl$^{-/-}$ transfected with β3-wt GFP integrin (green) and Vcl mCherry (red). (G) Quantifications of colocalization of β3-wt GFP with Fn for cells treated as described in A–C (control+FCS, *n*=66, *N*=3; control+DMSO, *n*=46, *N*=3; +10 μM blebbistatin, *n*=40, *N*=3; +10 μM Y-27632, *n*=54, *N*=3; +NMIIA mCherry, *n*=55, *N*=3). (H) Quantifications of colocalization of β3-wt GFP with Fn for cells treated as described in D–F (control, *n*=38, *N*=3; MEF Vcl$^{-/-}$, *n*=57, *N*=3; MEF Vcl$^{-/-}$+Vcl mCherry, *n*=42, *N*=3). Fluorescent images in A–F were acquired with SR-SIM. White dashed lines indicate cell outline. Scale bars: 10 μm in overview images, 2 μm in zoom-ins.

We conclude that our MD simulations, performed without mechanical pull on the β3 integrin, reflected the structure of β3-N305T integrin in experiments with contractility inhibition (Fig. 3E,G). We propose that αVβ3 integrin needs mechanical load for its final activation with maximal hybrid domain swing-out. Only this αVβ3 integrin conformation seems to be able to stably bind Fn in a cellular environment.

### Extended-open conformation of αVβ3 integrin is not necessary for Vn binding

Our experiments indicated that stable Fn binding by αVβ3 integrin requires force-dependent hybrid domain swing-out. In contrast, αVβ3 integrin was able to bind Vn in experiments in which cell contractility was reduced. Accordingly, we wanted to test whether αVβ3 integrin can bind Vn already in the extended-closed conformation. To this end, we set out to develop an integrin mutation locking αVβ3 integrin in the extended-closed conformation. We created a disulfide bridge between the βI-like and the hybrid domain of β3 integrin to limit the degree of the hybrid domain swing-out (β3-V80C/D241C). Structural analysis supported our rationale for this mutation (Fig. 4A). We prepared a model, where cysteine mutations were introduced into the extended-closed conformation of αVβ3 integrin (PDB: 4MMX) using PyMOL and energy minimization of the model. The disulfide

Journal of Cell Science (2020) 133, jcs242404. doi:10.1242/jcs.242404

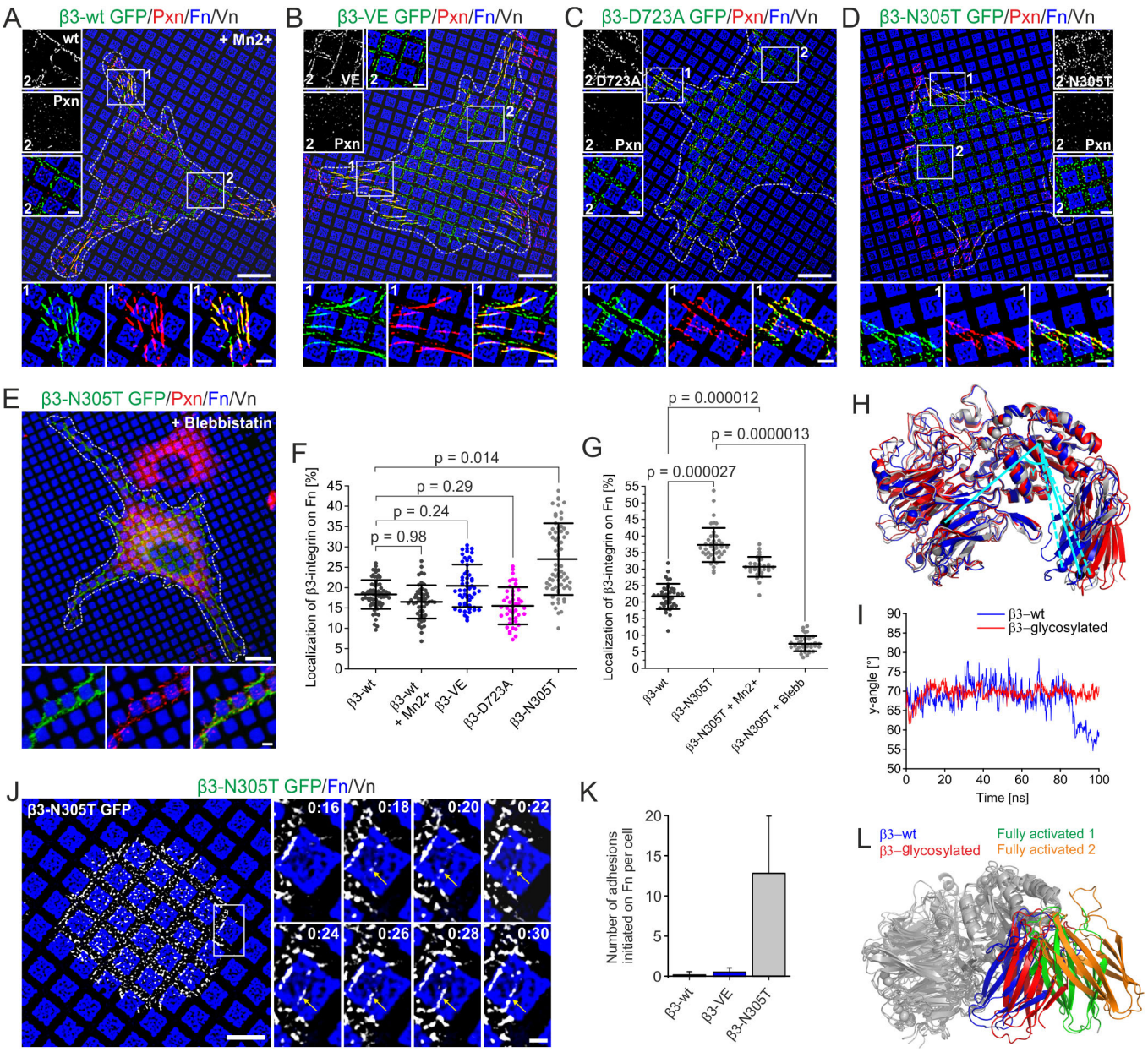


**Fig. 3. Hybrid domain swing-out is necessary for αVβ3 integrin binding to FN.** (A) NIH3T3 cell transfected with β3-wt GFP integrin (green). 1 mM $Mn^{2+}$ was added to the medium 30 min before fixation. (B–D) NIH3T3 cell transfected with β3-VE GFP integrin (green) (B), β3-D723A GFP integrin (green) (C) or β3-N305T GFP integrin (green) (D). (E) β3-N305T GFP integrin-transfected cells treated with 10 µM blebbistatin. All cells (A–E) were fixed and immunostained for paxillin (Pxn; red). Zoom-ins depict adhesions in the cellular periphery (1) or the cell center (2). (F) Quantifications of colocalization of β3 GFP with Fn for cells treated as described in A–D and imaged with SR-SIM. Paxillin was used as a mask to exclude αVβ3 integrin clusters in the cell center from analysis (β3-wt is a replot of the data from Fig. 1D; β3-wt+Mn2+, *n*=55, *N*=3; β3-VE, *n*=54, *N*=3; β3-D723A, *n*=43, *N*=3; β3-N305T, *n*=66, *N*=4). (G) Quantification as described in F for cells treated as described before. Data for 'β3-N305T+Mn2+' were acquired from cells treated as described in D but with addition of 1 mM $Mn^{2+}$ for the last 30 min before fixation. All images were acquired with diffraction-limited microscopy (β3-wt, *n*=40, *N*=3; β3-N305T, *n*=42, *N*=3; β3-N305T+Blebb, *n*=39, *N*=3). (H) Superimposition of the initial structure of αVβ3 integrin (gray), the same structure after 100 ns molecular dynamics (MD) simulation (blue) and the N303-glycosylated structure after 100 ns MD simulation (red). Cyan lines indicate the position of hybrid domain swing-out measurements. (I) Fluctuation of the angle γ between βI-like and hybrid domain over time during the MD simulation. (J) Live-cell SR-SIM imaging of a NIH3T3 cell transfected with β3-N305T GFP integrin (white) spreading on Fn/Vn substrates (Fn in blue). Yellow arrows indicate an αVβ3 integrin-mediated adhesion that initiated on Fn. (K) Number of αVβ3 integrin-mediated adhesions per cell that initiated on Fn for NIH3T3 cells transfected with the indicated integrin (β3-wt is a replot of the data in Fig. 1I; β3-VE, six cells analyzed out of three independent experiments; β3-N305T, six cells analyzed out of four independent experiments). (L) Superimposition of αVβ3 integrin structures as described in H for β3-wt (blue) and β3-glycosylated (red). Fully activated structures were created based on PBD: 4MMX with an arranged hybrid domain swing-out according to PBD: 3EZ2 (Fully activated 1, green) or PBD: 3FCU (Fully activated 2, orange). Scale bars: overview images 10 µm, zoom-ins 2 µm. White dashed lines indicate cell outline. Images were acquired with SR-SIM (A–D,J) or diffraction-limited microscopy (E).

bridge caused only minimal distortion of the protein; the distance between Cα atoms of V80C and D241C after introducing a disulfide bond did not change compared to the wild-type situation (for both structures d=6.3 Å). In contrast, αVβ3 integrin in the extended-open conformation showed an increased distance by a factor of three (d=19.4 Å) between Cα atoms of V80 and D241, implying that a

Journal of Cell Science (2020) 133, jcs242404. doi:10.1242/jcs.242404

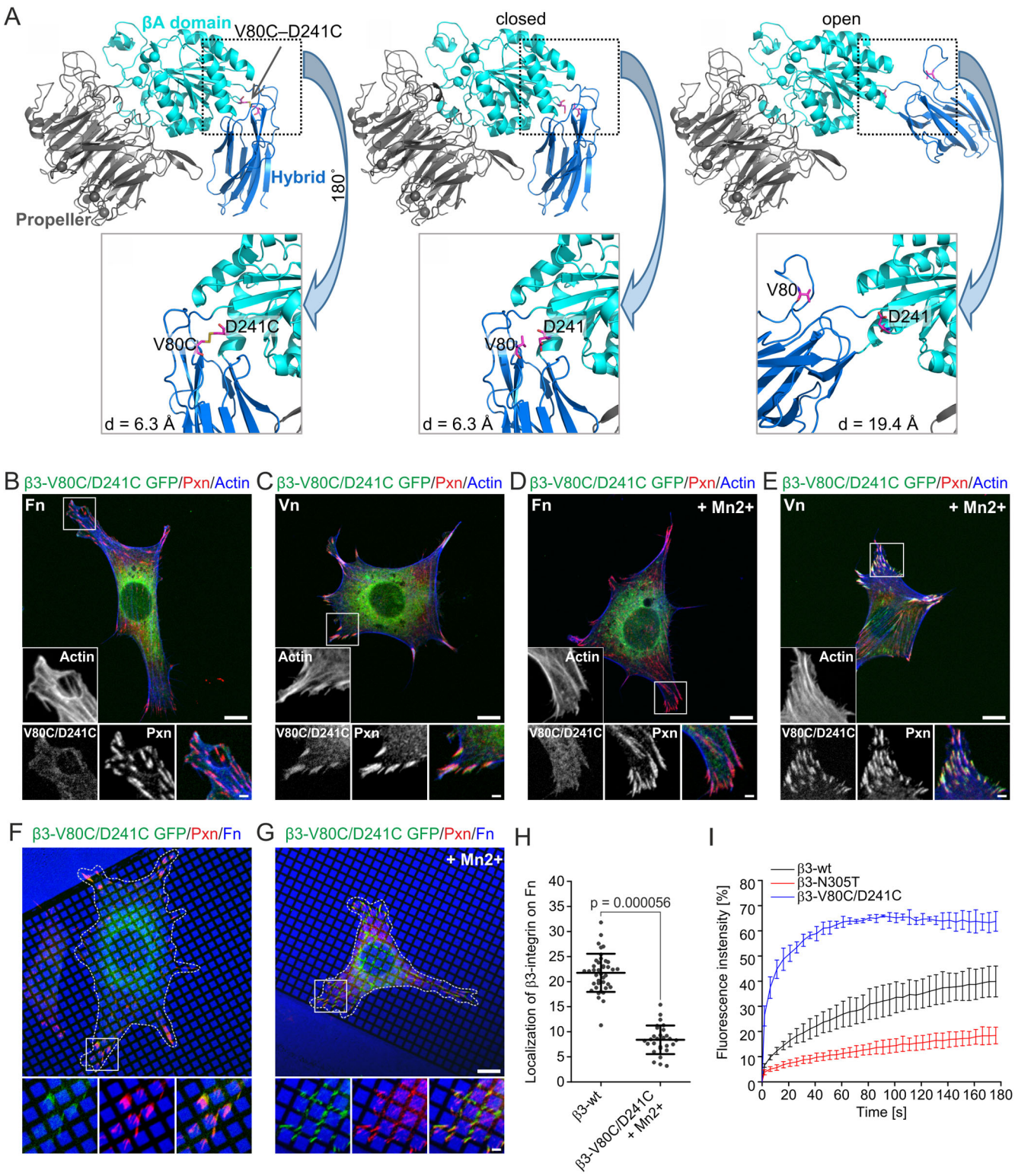


**Fig. 4. Extended-closed mutant β3-V80C/D241C binds Vn but not Fn.** (A) Structural analysis of the distance between V80 and D241 for extended-closed conformation of αVβ3 integrin (left; PBD: 4MMX) after introducing a V80C/D241C disulfide bridge for the wt structure (middle), or for the extended-open conformation (right; PBD: 4MMX; hybrid domain swing-out arranged based on PBD: 3FCU). (B–E) NIH3T3 cells transfected with β3-V80C/D241C GFP (green) cultured on the indicated ECM proteins for 2 h. 1 mM $Mn^{2+}$ was added for the last 30 min where indicated. Cells were stained for paxillin (red) and actin (blue) after fixation. Please note the absence of αVβ3 integrin clustering on Fn and the increased localization of β3-V80C/D241C in adhesions on Vn for $Mn^{2+}$-treated compared to untreated cells. (F,G) Cells were prepared as described in B–E except that they were cultured on Fn/Vn substrates. (H) Quantifications of colocalization of β3 GFP with Fn for cells treated as described in G (β3-wt is a replot of the data from Fig. 3G; β3-V80C/D241C+Mn2+, *n*=29, *N*=3). (I) NIH3T3 cells were transfected with the indicated plasmids and cultured on serum-coated cover slips for 15–20 h. FRAP measurement of αVβ3 integrin dynamics for the indicated conditions (β3-wt, *n*=40, *N*=3; β3-N305T, *n*=48, *N*=3; β3-V80C/D241C, *n*=36, *N*=3). Scale bars: overview images 10 µm, zoom-ins 2 µm. White dashed lines indicate cell outline. Fluorescent images were taken with diffraction-limited microscopy.



Journal of Cell Science

Journal of Cell Science (2020) 133, jcs242404. doi:10.1242/jcs.242404

V80C-D241C disulfide bridge can block the transition to the extended-open conformation.

Next, we expressed β3-V80C/D241C GFP in NIH3T3 cells and cultured them on substrates homogenously coated with either Fn or Vn (Fig. 4B,C). On both substrates, we observed a high GFP background signal, potentially indicating that large amounts of β3-V80C/D241C cannot be recruited into adhesion sites. However, the GFP signal revealed a clustering of β3-V80C/D241C into adhesions on Vn but not at all on Fn. Treatment of cells with $Mn^{2+}$ increased the clustering of β3 V80C/D241C into adhesions on Vn but not on Fn (Fig. 4D,E). Adding 1 mM dithiothreitol (DTT) to open disulfide bridges allowed clustering of β3 V80C/D241C on Fn (Fig. S4A,B,E), confirming that the V80C/D241C disulfide bridge formed and that the conformation of β3-V80C-D241C prevents Fn binding. On Fn/Vn substrates, we observed weak β3-V80C/D241C GFP-positive adhesions that could not be reliably quantified due to the high background signal. However, a restricted localization of β3-V80C/D241C GFP on Vn was obvious (Fig. 4F). Since $Mn^{2+}$ treatment enhanced the recruitment of β3-V80C/D241C into adhesion sites only on Vn (Fig. 4D,E), ligand selection seems not to be influenced by $Mn^{2+}$ (as observed before; Fig. 3F). Thus, we treated β3-V80C/D241C GFP-expressing cells on Fn/Vn substrates with $Mn^{2+}$. We observed an enhanced clustering of β3-V80C/D241C GFP into adhesions, while still preserving the restriction to Vn (Fig. 4G,H). This increased fluorescence signal allowed a reliable quantification and revealed a significantly reduced localization of β3-V80C/D241C on Fn (8.4% colocalization with Fn; optical sectioning microscopy) compared to β3-wt integrin (21.8% colocalization with Fn; optical sectioning microscopy). We analyzed β3-V80C/D241C and β3-wt-expressing cells on Fn/Vn substrates also in the presence of 1 mM DTT (Fig. S4C,D,F) and observed increased Fn localization of β3-V80C/D241C treated with DTT. In contrast, β3-wt showed no change in Fn localization due to DTT treatment (β3-wt, 21.8%; β3-wt+1 mM DTT, 22.3%; β3-V80C/D241C+1 mM $MnCl_2$, 8.4%; β3-V80C/D241C+1 mM DTT, 15.8%). A flow cytometry-based assay to measure β3 integrin activation (Pinon et al., 2014) confirmed these observations (Fig. S4G). Importantly, another disulfide bridge mutation locking the integrin in the inactive bent state [β3-V332C/S674C (Takagi et al., 2002)], showed significantly reduced β3 integrin activation in this assay. This supported our rationale that mutationally introduced disulfide bridges form and that they are stable in cell experiments, indicating that β3-V80C/D241C is indeed locked in a conformation as presented in Fig. 4A.

We further extended these data using the integrin inactivator $Ca^{2+}$ (Fig. S3C,D). Treatment of β3-wt GFP-expressing cells with $Ca^{2+}$ reduced Fn binding to a similar extent as inhibition of contractility or the β3-V80C/D241C mutation. We also compared the fluorescence recovery after photobleaching (FRAP) of β3-wt, β3-N305T and β3-V80C/D241C, in order to understand the influence of these mutations on αVβ3 integrin turnover in adhesions (Fig. 4I; Fig. S4H). Interestingly, β3-V80C/D241C GFP showed a very fast turnover compared to β3-wt GFP, while the turnover of β3-N305T GFP was slower than that of β3-wt GFP, confirming observations in B16F1 melanoma cells (Cluzel et al., 2005). In summary, we propose that αVβ3 integrin is not relying on the fully extended-open conformation to bind Vn, whereas Fn binding needs a conformational change to the extended-open conformation.

### Preference for Vn influences cell migration and mechanotransduction

Our results so far revealed a mechanism enabling αVβ3 integrin to differentiate between Fn and Vn based on the degree of the force-dependent hybrid domain swing-out. However, stable binding to any ligand might result in the fully active extended-open conformation of αVβ3 integrin irrespective of the actual ligand present. Therefore, it is possible that the preference of αVβ3 integrin for Vn compared to Fn is compensated on a cellular level when only one ligand is present. Thus, we performed additional experiments to test this hypothesis. First, we tested the dependency of αVβ3 integrin on mechanical force and hybrid domain swing-out for Fn binding on homogenous substrates. Therefore, we cultured β3-wt GFP- or β3-N305T GFP-expressing NIH3T3 cells on Fn-coated cover slips in the presence of different concentrations of Y27632 (Fig. S5E). This analysis confirmed that Fn is not an ideal ligand for αVβ3 integrin even when it is the only ligand present (Fig. S5F; also seen in Fig. S2). However, enforced hybrid domain swing-out (β3-N305T) supports stable adhesion formation of αVβ3 integrin on Fn. But, even in the context of the β3-N305T mutation, cell contractility is needed to support Fn binding as indicated by the Y27632-dependent reduction in adhesion size as shown before (Fig. 3E,G). Next, using live-cell imaging, we analyzed cell migration of β1 integrin-deficient GD25 cells on substrates homogeneously coated with either Fn or Vn. Cell tracking revealed that cells on Fn migrated almost two times faster ($v_{Fn}$=12.0±3.08 µm/h) compared to cells migrating on Vn ($v_{Vn}$=6.7±0.39 µm/h; Movie 7). To understand how cell behavior is influenced when GD25 cells can choose between Vn and Fn, we produced stripes of Vn/Fn with cellular resolution (Vn, 20 µm; Fn, 40 µm). Live-cell imaging for 12 h on these Fn/Vn stripes revealed a turning of cells away from Fn towards Vn (Fig. 5A; Movie 8). To quantify this behavior, we measured the surface area of single cells overlying Fn stripes at different time points (Fig. 5B). Thirty minutes after seeding, cells covered Fn- and Vn-coated surfaces according to the geometrical coverage (1/3 Vn, 2/3 Fn), indicating a random distribution (Fn/cell colocalization, 67.5%). With increasing time, the surface area of single cells colocalized less with Fn (Fn/cell colocalization after 8 h, 28.4%; 24 h, 14.6%), demonstrating a preference to adhere to Vn.

Additionally, we asked whether mechanosensing of the extracellular rigidity is affected by the force-dependent ligand binding of αVβ3 integrin. We cultured GD25 cells for 6 h on hydrogels with variable stiffness and homogeneously coated with Fn or Vn (Fig. 5C). We measured cell area and the length of paxillin-stained adhesions. Both ligands caused a similar sigmoidal increase in cell area and adhesion length with increasing hydrogel stiffness (Fig. 5D,E). However, cells on Vn showed adhesion maturation and enhanced cell spreading already at 6.7 kPa. Cells on Fn only reached similar plateau values for both parameters at substrates stiffer than 6.7 kPa.

To summarize, we observed that cellular behavior is regulated by the extracellular ligand of αVβ3 integrin. Cell migration and ligand selection experiments indicated that ligand preferences of αVβ3 integrin impact cell behavior and migration. In addition, mechanosensing and mechanotransduction is ligand dependent, implying that force-dependent ligand binding of αVβ3 integrin on Fn substrates requires higher stiffness of the microenvironment than binding of αVβ3 to Vn.

### Force-dependent ligand binding is not limited to αVβ3-Fn binding

αVβ3 integrin has been reported to be a highly promiscuous receptor that binds to other ligands besides Fn and Vn, such as fibrinogen (Fbg), Opn and thrombospondin (Tsp) (Humphries et al., 2006). We therefore produced binary-choice substrates to challenge αVβ3 integrin with either Vn/Fbg, Vn/Opn, Vn/Tsp or Opn/Fn

Journal of Cell Science (2020) 133, jcs242404. doi:10.1242/jcs.242404

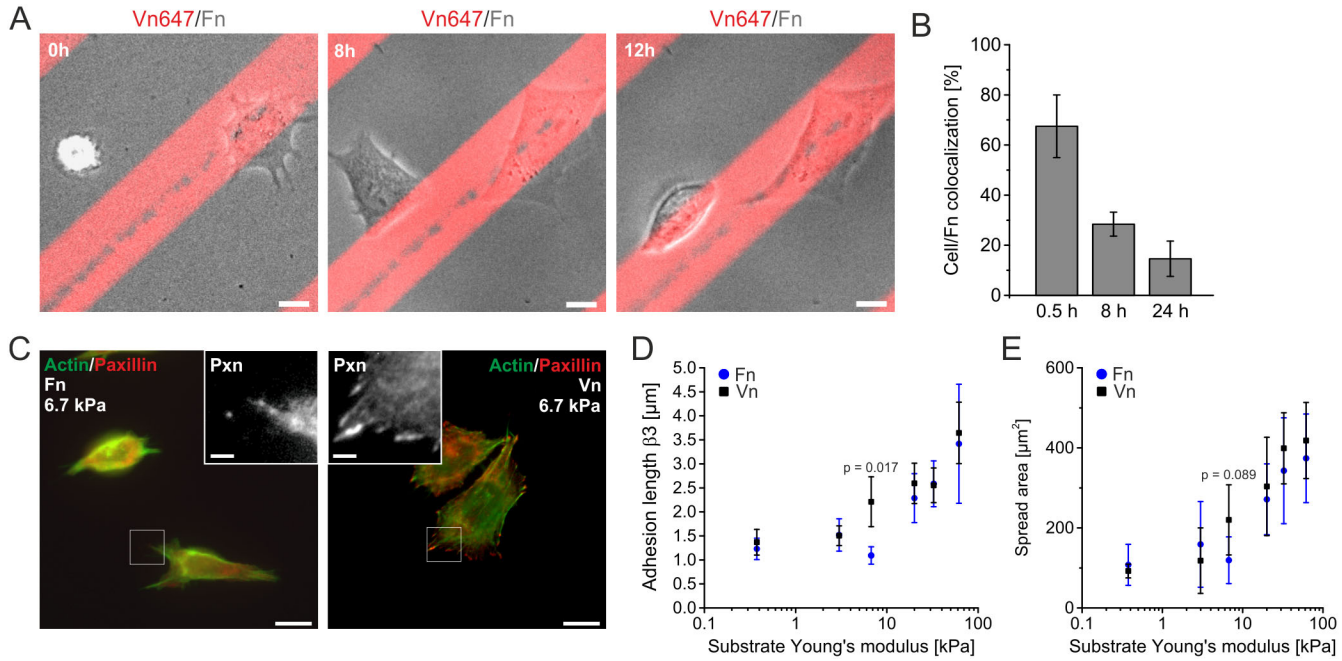


**Fig. 5. The preference of αVβ3 integrin for Vn influences cellular behavior.** (A) GD25 cells (no β1 expression) were seeded onto stripe assays of stamped Vn (red; 20 µm) backfilled with Fn (40 µm). Alexa Fluor 647-labeled Vn was added to visualize Vn stripes. GD25 cells were visualized with phase-contrast microscopy for 12 h. (B) Quantification of the colocalization of GD25 cells with Fn on Vn/Fn stripe assays at the indicated time points. The first time point was quantified based on phase-contrast movies as shown in A; 8 h and 24 h time points were calculated from experiments with cells cultured in the incubator, fixed and stained for actin (0.5 h, *n*=123, *N*=3; 8 h, *n*=17, *N*=3; 24 h, *n*=15, *N*=3. (C–E) GD25 were cultured for 6 h on polyacrylamide gels of the indicated Young's modulus (E) and stained for paxillin (red) and actin (green). Gels were coated homogeneously with Vn or with Fn. (C) Cells on 6.7 kPa hydrogels showed less cell spreading and adhesion maturation on Fn coated substrates compared to Vn. (D,E) Length of paxillin-stained adhesions (longest 10% only to indicate matured adhesions) (D) or cell area (E) was plotted against the Young's modulus for cells on Vn (black data points) or Fn (blue data points; see Table S1 for number of analyzed cells; *P*>0.1 except where indicated; see also Table S2). All cells were imaged with diffraction-limited microscopy. Scale bars: 10 µm in overviews, 2 µm in zoom-ins.

(Fig. S5A–D). On Vn/Fbg and Vn/Tsp, αVβ3 integrin preferred to form adhesions on Vn and only revealed 14.7% colocalization to Fbg (Fig. 6A) and 6.7% to Tsp (Fig. 6C). In contrast, on Vn/Opn substrates, no preference of αVβ3 integrin for one of the ligands could be detected (colocalization to Opn 50.4%; Fig. 6B). Finally, on Fn/Opn substrates, Opn is the preferred binding partner for αVβ3 integrin (colocalization to Opn 81.8%; Fig. 6D) as was the case with Vn on Fn/Vn substrates. Thus, in the context of binary-choice substrates, Opn resembled the preferred αVβ3 integrin ligand Vn and Fbg phenocopied Fn, while Tsp is not a proper ligand for αVβ3 integrin in this context.

## DISCUSSION

We have analyzed the interaction of αVβ3 integrin with different ligands by using Fn/Vn binary-choice substrates with subcellular geometry, different αVβ3 integrin mutants and altering cellular contractility. We observed that αVβ3 integrin binds preferentially to Vn under a wide range of conditions, while Fn binding required higher cellular contractility. Analyzing different αVβ3 integrin mutations that affect β3 conformation showed that (1) β3-V80C/D241C – interpreted to be locked in extended-closed – binds only Vn and thereby phenocopies αVβ3 integrin in low force conditions; (2) activating conditions favoring talin association (β3-D723A, β3-VE) do not shift the ratio of Fn/Vn binding; and (3) constitutive headpiece opening (β3-N305T+cellular contractility) increases Fn binding. Thus, we introduce a model in which mechanical load on αVβ3 integrin induces a full hybrid domain swing-out to the extended-open conformation via an intermediate extended-primed state (Fig. 6E). During this transition, αVβ3 integrin becomes gradually less selective/more promiscuous by accepting additional ligands like Fn and Fbg. We further show that these ligand-binding properties modulate cellular behavior during spreading, migration and mechanotransduction, depending on the respective ECM protein.

### The Vn receptor under force

The interaction between αVβ3 integrin, α5β1 integrin and Fn is intensively studied in different pathological situations and is relevant for morphogenesis (Benito-Jardón et al., 2017; Brunner et al., 2011; van der Flier et al., 2010; Yang et al., 1999). However, αVβ3 was initially described as the 'Vn receptor' because of its high Vn-binding properties and, equally important, its inability to bind to Fn (Pytela et al., 1985). How can these contradictory results for αVβ3 integrin be explained? Indeed, under low-force conditions (Fig. 2; Fig. S3F–I), αVβ3 integrin shows high selectivity for Vn and seemingly is the 'Vn receptor'. However, the ability of αVβ3 to bind Fn is enhanced by cellular contractility (Fig. 2C,G). This might explain the abundant examples of αVβ3 integrin acting as an Fn receptor in culture (Elosegui-Artola et al., 2016; Roca-Cusachs et al., 2009; Schiller et al., 2013) or in organisms (Benito-Jardón et al., 2017; Takahashi et al., 2007; van der Flier et al., 2010), in contrast to the force-free assay initially used by Pytela and colleagues (Pytela et al., 1985). All experiments presented here indicate, however, that αVβ3 integrin is rather an auxiliary Fn receptor (at least under cell culture conditions). Yet, this might be a prerequisite for different cellular tasks of αVβ3 and α5β1 integrin in the presence of Fn (Roca-Cusachs et al., 2009; Schiller et al., 2013).

Journal of Cell Science (2020) 133, jcs242404. doi:10.1242/jcs.242404

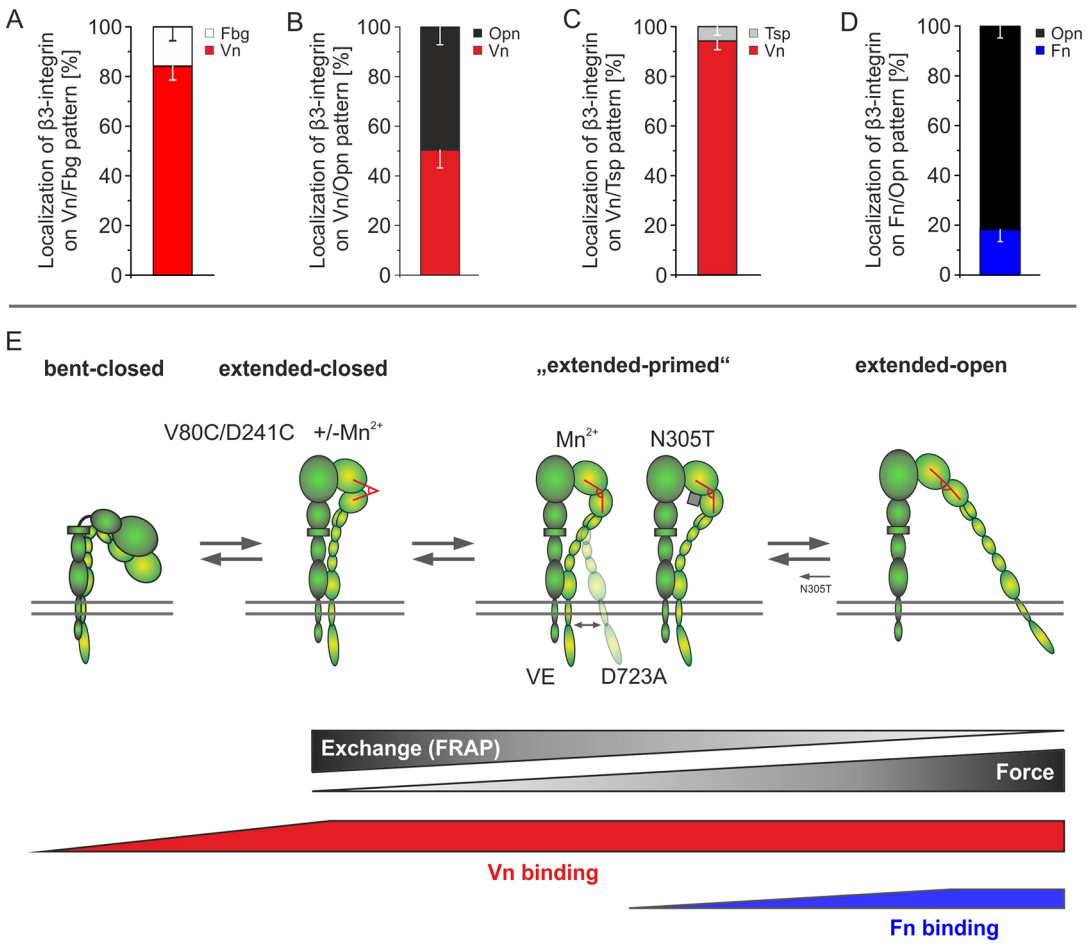


**Fig. 6. Osteopontin (Opn) phenocopies Vn, fibrinogen (Fbg) phenocopies Fn in binary-choice substrates.** (A–D) β3-wt GFP was expressed in NIH3T3 cells that were cultured on alternative binary-choice substrates (Fig. S5A–D). Quantification of the colocalization of β3-wt GFP with indicated ECM proteins for cells cultured on Vn/Fbg ($n$=57, $N$=3), Vn/Opn ($n$=45, $N$=3), Vn/Tsp ($n$=34, $N$=3) or Fn/Opn ($n$=53, $N$=3). (E) Model for force-dependent differential ligand binding of αVβ3: αVβ3 integrin is in equilibrium between bent and extended conformations. Integrin mutations may stabilize the integrin in intermediate conformations identified in a multistep activation process [for example, β3-N305T without force, step 7 of 8 (Zhu and Springer, 2013); N303-glycosylation, gray square between βI and hybrid domain]. Headpiece opening (indicated with red angle) is decisive for Fn binding, while Vn stays the preferred αVβ3 integrin ligand. Binding of Vn presumably precedes force-mediated headpiece opening that requires a ligand-integrin-actin axis to act on αVβ3 integrin. FRAP measurements indicate that low FRAP dynamics facilitate Fn binding (low off-rate of β3-N305T indicated by smaller equilibrium arrow from extended-open back to -primed). Thus, mechanical forces favor the full αVβ3 integrin activation that enables stable binding to additional ligands and thereby enhances ligand promiscuity of αVβ3 integrin.

Changes in adapter recruitment during adhesion maturation might be an alternative explanation for changes in ligand binding by αVβ3 integrin. Indeed, manipulation of intracellular contractility not only affects force transmission to single integrins but also adhesome composition (Kuo et al., 2011; Schiller et al., 2011). In fact, we showed that vinculin recruitment is needed for increased Fn-binding of αVβ3 integrin. However, to date, vinculin is best characterized as a transmitter of force from actin to the talin-integrin axis (Elosegui-Artola et al., 2016; Humphries et al., 2007; Rahikainen et al., 2017). Additionally, recruitment of adhesome proteins to focal adhesions seemed rather unaffected by vinculin knockout (Thievessen et al., 2013). Therefore, we conclude that the effect of vinculin in our experiments is best explained by its role as a force-transmitter. At the same time, we observed that Fn-binding properties of αVβ3 integrin under different force regimes strongly correlate with defined integrin mutations: low mechanical load – extended-closed conformation (β3-V80C/D241C); high mechanical load – extended-open conformation (β3-N305T+force) (Fig. 6E). Both of these mutations are extracellular, thereby limiting the potential effects on adapter recruitment. Thus, we propose that force transmission through αVβ3 is necessary for Fn binding.

### Structural insights into αVβ3 integrin activation

What is the active (ligand-binding) conformation of integrins? Recent studies reported for α5β1 integrin an affinity increase from extended-closed to -open conformation by 4000- to 6000-fold (Li et al., 2017). This difference makes it likely that the extended-closed conformation of α5β1 integrin is transient and switches directly to extended-open conformation in the presence of ligands. However, this might be different for other integrin receptors. In fact, αIIbβ3 integrin is reported to have an extended-closed/open affinity difference of ‘only’ 200-fold (Zhu and Springer, 2013). Moreover, the binding of soluble RGD peptides to αIIbβ3 and αVβ3 integrins in extended-closed conformation has been demonstrated in crystal structures (Xiong et al., 2002; Zhu and Springer, 2013). Using a new mutation (β3-V80C/D241C), we provide experimental evidence that αVβ3 integrin in the extended-closed conformation can bind Vn in a cellular environment. Importantly, our observations for αVβ3 integrin are in line with

Journal of Cell Science (2020) 133, jcs242404. doi:10.1242/jcs.242404

reports about integrin-ligand binding in conformations different from the extended-open state for other integrins [β2 to ICAM (Fan et al., 2019, 2016); αVβ3 to Thy1 (Fiore et al., 2015); αIIbβ3 to Fbg (Chen et al., 2019); α4β7 to MadCAM-1/VCAM-1 (Wang et al., 2018)]. Thus, it appears that the structure-function relationship of integrins can differ from that of α5β1 integrin. More structural integrin work, potentially with cryo-electron microscopy, avoiding spatial restrictions of a crystal environment, will help to test this hypothesis.

The need of αVβ3 integrin for complete hybrid domain swing-out in order to bind Fn might also explain the limited effect of classical integrin activators like $Mn^{2+}$, unclasping the integrin subunits (β3-D723A) or enhancing talin binding (β3-VE; 20-times higher affinity) on changing ligand preference by αVβ3 integrin. It is noteworthy that talin-head binding alone caused integrin extension but not headpiece opening (Ye et al., 2010). The literature for the conformational effects of $Mn^{2+}$ on β3 conformation appears more diverse with findings that $Mn^{2+}$ does not cause headpiece opening at all (Dai et al., 2015), only to 14% (Eng et al., 2011), or for the vast majority of β3 integrins (Miyazaki et al., 2018). Our data would support a limited effect of $Mn^{2+}$ on headpiece opening and fits best to studies using integrins including their natural transmembrane domains (Dai et al., 2015; Eng et al., 2011). Additionally, results from FRAP experiments correlate with our observations on Fn/Vn substrates: β3-D723A mutation and $Mn^{2+}$ treatment of β3-wt showed the same FRAP dynamics as β3-wt alone (Cluzel et al., 2005), in contrast to mutations that had an effect on the headpiece opening and on Fn binding (β3-N305T, β3-V80C/D241C, Fig. 4I). Activation by $Mn^{2+}$, β3-D723A or β3-VE might instead favor integrin extension and induce a primed state of αVβ3 integrin (Chen et al., 2019; Takagi et al., 2002), but without directly enforcing maximal hybrid domain swing-out.

### Regulation of ligand selection

How can αVβ3 integrin select between different ligands that all bind via the RGD sequence (Fn, Vn, Opn, Fbg, Tsp)? The conformation of RGD peptides clearly impacts integrin selectivity, given that cyclic RGD is selective for αVβ3 integrin, while linear RGD almost equally binds integrin receptors for Fn and Vn (Pierschbacher and Ruoslahti, 1987). Cormier and colleagues recently argued that ligand binding by αVβ3 integrin might not only be regulated by affinity, but also by the accessibility of the ligand to the binding pocket in the integrin headpiece (Cormier et al., 2018). Interestingly, the RGD motif of Fn is positioned in a rather short loop, while Vn and Opn seem to present this motif in a flexible, unstructured protein region. Thus, the limited flexibility of the RGD motif in Fn might cause constraints in accessibility to the binding pocket of αVβ3 integrin dependent on the integrin conformation.

A promiscuous receptor like αVβ3 integrin might encounter potential ligands *in vivo* most of the time. Accordingly, αVβ3 integrin-expressing cells might especially benefit from additional ways to regulate ligand binding and selection. So far, we have demonstrated a force-dependent recognition of Fn by αVβ3 integrin. Fittingly, αVβ3 integrin – in contrast to α5β1 integrin – is unable to bind soluble Fn (Danen et al., 2002). At the same time, αVβ3 integrin binds Opn from the medium, preventing anoikis in melanoma cells (Geissinger et al., 2002). It will be interesting to test additional physiological ligands concerning their dependency on physical parameters such as matrix anchorage, solubility or stiffness for binding to αVβ3 integrin. Influence of these physical parameters on ligand binding will clearly have an impact on pathological settings with altered tissue mechanics, such as fibrosis, wound healing or cancer.

### Consequences of force-dependent ligand selection

Knockout mice for Fn and for α5 integrin have similar phenotypes [death at embryonic day (E)8–8.5 or E9–9.5 (Yang et al., 1999)], indicating that α5β1 integrin is the main Fn receptor during development. In contrast, knockout mice for β3 are viable and fertile [despite showing increased mortality (Hodivala-Dilke et al., 1999)]. However, in certain settings, αV integrins and αVβ3 in particular are able to compensate for a loss of α5β1-Fn interaction (Benito-Jardón et al., 2017; Takahashi et al., 2007; van der Flier et al., 2010). Endothelial cells depleted in α5 integrin, for example, show increased recruitment of αV integrins to Fn fibers (van der Flier et al., 2010). It will be compelling to test whether such an increased recruitment of αVβ3 after α5 reduction is accompanied by increased contractility and/or changed morphology and altered mechanical characteristics of Fn fibers. Interestingly, AFM studies showed that early fibrillogenesis starts already in the cell periphery (Gudzenko and Franz, 2015) where αVβ3 is mostly localized and where high adhesive forces are detected (Kronenberg et al., 2017). Moreover, cancer-associated fibroblasts were reported to reorganize Fn in a multistage process during cancer spheroid invasion, with α5β1 and αVβ3 integrin having separate and distinct functions in this process (Attieh et al., 2017; Erdogan et al., 2017). On the other hand, Vn-binding by αVβ3 integrin is an important part of wound healing and inflammation (Keasey et al., 2018), supporting the relevance of ligand selection by αVβ3 integrin. Thus, we expect that force-dependent regulation of ligand promiscuity supports switching between different cellular functions for which we here present a first framework. Combining experiments with controlled presentation of ligands in 2D and 3D (Richter et al., 2017) and experiments mimicking tissues (Franco-Barraza et al., 2016; Kaukonen et al., 2017) will be important next steps to understand ligand selection by αVβ3 integrin in more detail.

## MATERIALS AND METHODS

### Cell culture, constructs and transfection

NIH3T3 cells used in this study are a subclone of NIH3T3 cells (American Type Culture Collection, CRL-16589) that were fluorescence-activated cell sorted for low expression of endogenous β3 integrin as described previously (Pinon et al., 2014). MEF $Vcl^{-/-}$ and MEF wt were kindly provided by W. H. Ziegler (Mierke et al., 2010). GD25 wt cells were kindly provided by R. Fässler (Wennerberg et al., 1996). All cells were grown at 37°C with 5% $CO_2$ in Dulbecco's modified Eagle medium (DMEM; Thermo Fisher Scientific) supplemented with 10% fetal calf serum (FCS; Hyclone), and passaged two to three times a week, or upon reaching confluency. Transfections were carried out with Lipofectamine 2000 Thermo Fisher Scientific) or JetPEI (Polyplus) according to the manufacturer's instructions. Cells were cultured in complete medium for 48 h before detachment. cDNA encoding full-length mouse β3-wt GFP integrin expressed in a cytomegalovirus promoter-driven pcDNA3/EGFP vector has been previously described (Ballestrem et al., 2001). β3-VE GFP (Pinon et al., 2014), β3-D723A GFP (Ballestrem et al., 2001) and β3-N305T GFP (Ballestrem et al., 2001) were derived by substitution from the β3-wt GFP integrin construct mentioned before and as described in the indicated publications. Vinculin mCherry was a gift from Christoph Ballestrem (Division of Cell Matrix Biology & Regenerative Medecine, University of Manchester, UK), and mApple-MyosinIIA-C-18 was Addgene plasmid #54929, deposited by Michael Davidson.

### Antibodies and chemicals

Inhibition experiments were performed with blebbistatin (Sigma-Aldrich), with the ROCK inhibitor Y27632 (Sigma-Aldrich), or with the αVβ3

Journal of Cell Science (2020) 133, jcs242404. doi:10.1242/jcs.242404

integrin inhibitor cilengitide (Sellekchem) at concentrations as indicated. DTT (Carl Roth) was used at the indicated concentration to open disulphide bridges. Cells were fixed for subsequent immunostaining with 4% paraformaldehyde (Sigma-Aldrich) in PBS. Reagents used for immunostaining were monoclonal mouse antibodies against paxillin (1:1000; clone 349/Paxillin, BD Biosciences, 610052), talin (1:100; clone 8d4, Sigma-Aldrich, T3287), vinculin (1:500; clone hVIN-1, Abcam, ab11194) and Vn (1:1000, clone VIT-2, IgM, Sigma-Aldrich, V7881), or polyclonal rabbit antibodies against hemagglutinin (HA)-tag (1:200; Sigma-Aldrich, H6903), Fn (1:500; Sigma-Aldrich, F3648), Tsp (1:100; Abcam, ab85762) or Opn (1:500; GeneTex, GTX37582). β1 integrin was stained with a monoclonal rat antibody (1:100; clone 9EG7, BD Biosciences, 553715). After primary antibody staining, samples were washed and incubated with antibodies against mouse labeled with Cy3 (1:500; Jackson ImmunoResearch, 115-165-146), against rabbit labeled with Alexa Fluor 488 (1:500; Thermo Fisher Scientific, A11070) or Cy3 (1:500; Dianova, 111-165-144), or with phalloidin coupled to Alexa Fluor 568 (1:200; Thermo Fisher Scientific, A12380). To visualize anti-Vn staining, secondary antibodies against IgM labeled with Cy3 were used (1:1000; Dianova, 115-166-075). Primary rat antibodies were visualized with pre-adsorbed, Alexa Fluor 488- or Alexa Fluor 568-labeled secondary antibodies (1:500; Thermo Fisher Scientific, A11006 or A11077) and, if present in the experiment, primary mouse antibodies were visualized with pre-adsorbed, Cy3-labeled antibodies (1:500; Dianova, 111-165-144) to avoid cross-reactivity of secondary antibodies. Direct labeling of Fn, Fbg and Vn was performed according to the manufacturer's protocol with Alexa Fluor 568 (Thermo Fisher Scientific, A10238) or Alexa Fluor 647 (Thermo Fisher Scientific, A20173).

### Microcontact printing

Silicone stamps for microcontact printing of differential substrates were produced as previously described (Lehnert et al., 2004). Binary-choice substrates were produced with human plasma Fn (Sigma-Aldrich, F2006 or Millipore, FC010), human plasma Vn (Sigma-Aldrich, V8379), recombinant human Vn (Sigma-Aldrich, SRP3186), native human Fbg (Bio-Rad, 4440-8604) or recombinant human thrombospondin-1 (R&D Systems, 3074-TH-050), or with Opn from bovine milk (Sigma-Aldrich, O3514).

For Fn/Vn substrates, silicone stamps were incubated for 10 min with a solution containing: (1) Alexa Fluor 647-labeled Fn (Fn-647; depending on labeling degree; typically, 2.5–3 µg/ml was used), (2) 5 µg/ml Fn and (3) 45 µg/ml heat-inactivated Fn in PBS (Fn-X; see Fig. S1E). Heat-inactivated Fn was produced by heating Fn for 30 min to 90°C. Cells do not spread on heat-inactivated Fn (Fig. S1E). After nitrogen drying of the stamp with the adsorbed Fn, the stamp was pressed onto a glass cover slip for 10 min before the stamp was released. Next, the pattern on the cover slip was covered with Vn at a concentration of 1–5 µg/ml in PBS for 1 h at room temperature. High concentrations of the stamped protein (Fn in this case, with 50 µg/ml total Fn+2.5–3 µg/ml Fn-647) improved the reproducibility of the patterns by preventing adsorption of the backfilled protein (Vn in this case) to the stamped areas.

For other binary-choice substrates than Fn/Vn, a total concentration of 50 µg/ml of the stamped protein and 5 µg/ml of the backfilled protein was used. The only exception is the Vn/Fn stripe pattern shown in Fig. 5A, where 10 µg/ml for both proteins was used. All other steps for stripe patterns were performed as described. After the final incubation step, patterns were washed with PBS and used directly for cell seeding. Cell detachment from culture flasks was stopped with trypsin inhibitor (Sigma-Aldrich) and cells were cultured in the absence of FCS if not stated otherwise. However, Fig. 2G indicated that FCS adsorption was negligible on Fn/Vn patterns during a 2 h incubation period.

### Polyacrylamide gels

Established protocols (Kandow et al., 2007; Pinon et al., 2014; Plotnikov et al., 2014) were adapted to gain polyacrylamide gels of different Young's modulus (stiffness) with homogeneous or with structured ECM. Gels were produced on activated cover slips: glass cover slips were cleaned with propanol and for 10 min in a plasma cleaner (Technics Plasma, Germany). This was followed by a silanization [1 h at room temperature, 1 mM 3-(trimethoxysilyl)propyl methacrylate (Sigma-Aldrich) in toluene]. After incubation, cover slips were washed in $ddH_2O$ and dried with nitrogen. On these cover slips, 60 µl of a mixture of degassed acrylamide, bisacrylamide (both Bio-Rad), tetramethylethylenediamine (TEMED) and ammonium persulfate (APS) (both Sigma-Aldrich) was pipetted with final concentrations of 0.5% APS, 0.1% TEMED and as mentioned in Table S1. This solution was covered with 10 µl of 1% w/v of acrylic acid *N*-hydroxysuccinimide ester (NHS acrylate; Sigma-Aldrich) in toluene. Finally, the solution was covered with a cover slip of 18 mm diameter that was either functionalized with a Fn/Vn pattern prepared as described before or that was coated with a 50 µg/ml solution of Fn or Vn for 1 h at room temperature. This top cover slip was dried with nitrogen before it was applied to the gel solution. After polymerization of the polyacrylamide gel, the top cover slip was removed and the gel was covered with PBS. Gel substrates were used directly for cell seeding or were stored overnight at 4°C before cell seeding. Cells were cultured for 6 h on gels in DMEM without FCS to prevent adsorption of plasma Vn to the gel surface.

Stiffness of polyacrylamide gels was measured as previously described (Elosegui-Artola et al., 2016). Measurements were performed with the atomic force microscope described below. Silicon nitride pyramidal tips with a nominal spring constant of k=0.01–0.03 $Nm^{-1}$ were used (MLCT, Bruker). An effective half-angle of 20° was used for calculation. For each stiffness, three gels from three independent batches were measured by probing five positions in the center of the gel with five repetitive measurements. The Hertz model equation for pyramidal tips was fitted to the force-displacement curves.

### Microscopy

SR-SIM imaging was performed on a non-serial Zeiss Elyra PS.1 microscope with a 63×/1.4 NA oil immersion objective and an Andor iXon EMCCD camera. The grid for SR-SIM was rotated three times and shifted five times leading to 15 frames of raw data out of which a final SR-SIM image was calculated with the structured illumination package of ZEN software (Zeiss). Values for calculation were selected for best resolution without causing image artefacts. Channels were aligned by using a correction file that was generated by measuring channel misalignment of fluorescent tetraspecs (Thermo Fisher Scientific, T7280). All diffraction-limited images, according to the figure legend, were taken using the ApoTome module on a Zeiss AxioimagerZ1 microscope to achieve optical sectioning. A 63×/1.4 NA oil immersion objective and a Zeiss AxioCam MRm were used. For SR-SIM live-cell microscopy, the incubation chamber was heated to 37°C and cells were imaged every minute. During imaging, cells were cultured in imaging medium (F12+25 mM HEPES+200 mM L-glutamine+1% penicillin/streptomycin, pH 7.2). FCS was present as indicated in the description for Movies 1–8. SR-SIM raw data images were processed as described above. Phase-contrast live-cell imaging was performed on a Zeiss Axio-Observer Z.1 with a 20×/0.8 NA air objective. Cell migration of GD25 cells on homogenous Fn or Vn (coating, 10 µg/ml in PBS for 1 h at room temperature) was analyzed for cells cultured in DMEM/F12 medium (Thermo Fisher Scientific, 11039-021)+1% penicillin/streptomycin+1% FCS. Migration of GD25 cells on Vn/Fn stripes was analyzed for cells cultured in DMEM/F12 medium+1% penicillin/streptomycin.

### FRAP

FRAP was performed as described previously (Wehrle-Haller, 2007). Image acquisition and image analysis were performed at the Bioimaging Core Facility, Faculty of Medicine, University of Geneva. Briefly, transfected NIH3T3 cells were cultured on serum-coated coverslips. One hour before imaging, medium was replaced with F12 medium (Sigma-Aldrich) containing 10% FCS+1% penicillin/streptomycin and cells were relocated to the microscope. FRAP was performed on a Nikon A1r confocal laser scanning microscope equipped with a 60× oil immersion objective and a 37°C incubation chamber. Three pictures in 5 s intervals were acquired before bleaching. After that, one frame/5 s was acquired for 3 min. The graph was calculated in the following way: the first three images before bleaching were averaged to yield '100% intensity' and the first image after bleaching was set to '0% intensity'. All other values were calculated as ratio of 100% intensity.

### AFM

To prepare adhesion substrates for directly comparative adhesion force spectroscopy, adjacent areas on a Fluorodish 35 (WPI) glass-bottom dish were coated with 50 µg/ml bovine serum albumin (BSA; to provide low adhesion for cell capture, see below), 50 µg/ml Fn or 5 µg/ml Vn solutions and incubated for 1 h. Substrates were subsequently rinsed five times with PBS and transferred to $CO_2$-independent medium (Thermo Fisher Scientific). Prior to single-cell force spectroscopy experiments, GD25 cells were transferred to $CO_2$-independent medium for 1 h and then trypsinized. Trypsin was subsequently inactivated by adding soybean trypsin inhibitor (Sigma-Aldrich). After centrifugation, the supernatant was removed, and cells were again resuspended in $CO_2$-independent medium. Single-cell force spectroscopy experiments were performed using a CellHesion 200 atomic force microscope (JPK) featuring an extended vertical range of 100 µm. All measurements were performed at 37°C using a temperature-controlled sample chamber (BioCell from JPK) and tipless 205 µm-long V-shaped cantilevers with a nominal spring constant of 0.06 N/m (NP-O from Veeco). To facilitate cell capture, plasma-cleaned cantilevers were functionalized with concanavalin A. After calibrating the sensitivity of the optical lever system and determining the spring constant, cells were pipetted into the sample chamber. A single cell was captured above the BSA-coated area by pressing the functionalized cantilever onto the cell with a contact force of 500 pN for 3 s and elevating the cantilever subsequently. To measure cell detachment forces, the cantilever was lowered at a constant speed of 5 µm/s until the cell made contact with the substrate and a pre-set force of 1.5 nN was reached. Afterwards, the cantilever was held at a constant height for the pre-set contact time until the cantilever was elevated 80 µm above the substrate surface. Each cell was tested alternatingly on Fn and Vn surfaces (typically ten force cycle repetitions for each contact time) to determine the differential adhesion strength to both ligands. In total, eight different cells were tested. Detachment forces were analyzed using the JPK image processing software. From the collected force-distance curves, the maximum detachment forces (maximum cantilever deflection) were determined and plotted as mean±s.d. using OriginPro 8.1G. Statistical significance of experiments was tested with a Wilcoxon-based Mann–Whitney *U*-test using InStat.

### Image analysis

Colocalization, cell area and adhesion length were analyzed with the Fiji software package (Schindelin et al., 2015). A threshold was applied to the intensity of the corresponding fluorescent channel, and the area or the length of individual integrin-mediated adhesions was measured with plugins included in Fiji. If necessary, background was subtracted (sliding paraboloid) or analysis was limited to adhesions in areas with less background. Colocalization between two fluorescent channels was quantified by measuring Mander's coefficient of thresholded images by using the Fiji plugin JACoP (Bolte and Cordelieres, 2006). The location of adhesion initiation on Fn/Vn substrates was defined by analyzing SR-SIM live-cell movies. The fluorescent channel of the integrin staining was analyzed while the Fn channel was hidden. Integrin clusters visible for at least two subsequent time frames were marked with an ellipse in the ZEN imaging software throughout the movie. Afterwards, the Fn channel was uncovered, and the positions of all ellipses were counted with respect to Fn squares or Vn surrounding the squares. If an integrin cluster initiated at the border of a square with contact to Fn and Vn, it was counted for the category 'Fn/Vn'.

### Biolayer interferometry measurement

Binding and unbinding behavior of αVβ3 integrin binding to different ECM proteins was measured using the BLItz biolayer interferometer (Pall ForteBio). All steps during real-time measurements were performed at room temperature in the same buffer conditions (20 mM Tris-HCl, 150 mM NaCl, pH 7.4, 1 mM $MgCl_2$, 1 mM $CaCl_2$, 0.02% Tween 20, 0.1% BSA). Pre-hydrated (10 min in integrin buffer) Ni-NTA biosensors (Pall ForteBio) were loaded with 50 µg/ml His-tagged human recombinant αVβ3 integrin (R&D Systems, 3050-AV) following an association phase with 150 µg/ml ECM protein and a dissociation phase (time scheme: baseline, 45 s; loading, 180 s; baseline, 45 s; association, 300 s, dissociation, 250 s). Binding curves were corrected for a reference sample: an integrin-loaded biosensor was used without adding ligand in the association phase (to correct for drift of the system and unspecific bound buffer components). In control experiments (Fig. S3E), 20 µM cilengitide was added to the integrin buffer during dissociation phase. A 10 s adjustment step was included.

### MD simulations

The crystal structure of αVβ3 integrin from RCSB Protein Data Bank (PDB: 4MMX) was used as a model for the extended-closed integrin. Structure of the extended-open form was prepared by superimposition of βI-like and hybrid domains from the crystal structure of open αIIbβ3 integrin (PDB: 3FCU or PDB: 3ZE2, as indicated in the figure legend). Systems containing unliganded αVβ3 were prepared by removing the tenth domain of Fn (FnIII10) from the initial structure. Glycosylation of β3 integrin at N303 was achieved by covalently attaching four sugar rings to a nitrogen atom of the N303 residue. Preparation of structures and analysis was performed using PyMOL 1.7. MD simulations were performed using Gromacs ver 2016.5 (Van Der Spoel et al., 2005) at the Sisu supercomputer, CSC, Finland. The Amber ff99SB-ILDN force field (Lindorff-Larsen et al., 2010) and explicit TIP3P water model (Jorgensen and Madura, 1983) were used. The total system charge was neutralized with $K^+$ ions. The parameters for the glycosylation part were prepared using ACPYPE (Sousa da Silva and Vranken, 2012). Energy minimization of the system was performed in 25,000 steps using steepest descent algorithm. The system was equilibrated in three phases using harmonic position restraints on all heavy atoms of protein. The first phase of equilibration was performed for 100 ps using the Berendsen weak coupling algorithm (Berendsen et al., 1984) to control the temperature of the system at 100 K. An integration time step of 2 fs was used in all the simulations. Following NVT, the system is linearly heated from 100 K to 310 K over 1 ns using an NPT ensemble at 1 atm of pressure. During this process, the Berendsen algorithm was used to control both temperature and pressure. For the final phase of equilibration and for all subsequent simulations, an NPT ensemble was maintained at 310 K, using V-rescale algorithm (Bussi et al., 2007), and 1 atm, using Berendsen algorithm. Temperature coupling was applied separately for protein and solution parts.

### Flow-cytometric β3 integrin activation index

NIH3T3 cells were transfected with JetPrime (Polyplus) and the indicated β3 plasmids according to the manufacturer's protocol. Cells were detached after 48 h and split into two groups. One was stained with hamster anti-mouse β3 integrin (1:500; clone HMβ3-1, BD Biosciences, 550541) and goat anti-hamster phycoerythrin (1:600; Jackson ImmunoResearch, 127-115-160). The other group of cells was incubated with a fusion protein of CD31 (also known as Pecam1) and the RGD-containing ligand soluble Kistrin-7 (Ski7; used 1:5 as supernatant from cell culture), followed by staining for CD31 with rat anti-CD31 (1:50; clone GC51, supernatant) and goat anti-rat phycoerythrin staining (1:800; Jackson ImmunoResearch, 112-116-143). All reagents were diluted in PBS+1% BSA and incubations were performed for 30 min on ice. Cells were washed by centrifugation and resuspending of the pellet in fresh, ice-cold PBS 2× before every incubation and after the last incubation. Before cytometric analysis, cell pellets were resuspended in PBS+1% BSA+1 mM EDTA. All analyses were performed on an Accuri C6 and data were analyzed with FlowJo (BD Biosciences). After bleed-through correction and gating for viable, transfected single cells, median values of phycoerythrin staining were calculated for total β3 and Ski7-stained β3. The ratio of Ski7/total staining was calculated and normalized to the activation ratio of β3-wt GFP.

### Statistics

If not stated otherwise, reported values in bar charts are calculated as mean, and error bars represent s.d. of all data points. In box plots, upper and lower bars indicate s.d. and the middle bar indicates the mean. Statistical comparisons are calculated with two-tailed Student's *t*-test based on the number of independent experiments. For adhesion force measured with AFM, the statistical significance of experiments was tested with a Wilcoxon-based Mann–Whitney *U*-test using InStat. All experiments

were reproducible and were carried out as independent experiments at least twice or as often as indicated in the figure legends.

**Acknowledgements**
We thank Marc Hippler for help with AFM measurements, Melanie Merkel for help with the analysis of *de novo* clusters, and Deepthy Kavungal for help with cell migration assays and bioimaging. We acknowledge CSC – IT Center for Science for computational resources, and the flow cytometry core facility at the CMU, University of Geneva.

**Competing interests**
The authors declare no competing or financial interests.

**Author contributions**
Conceptualization: M. Bachmann, B.W.-H., M. Bastmeyer; Methodology: M. Bachmann, M.S., V.V.M., C.M.F., V.P.H., B.W.-H., M. Bastmeyer; Software: V.V.M., V.P.H.; Formal analysis: M. Bachmann, M.S., V.V.M., M.R., L.H., K.W., S.K., C.M.F., B.W.-H.; Investigation: M. Bachmann, M.S., V.V.M., M.R., L.H., K.W., S.K., C.M.F.; Resources: C.M.F., V.P.H., B.W.-H., M. Bastmeyer; Data curation: M. Bachmann, M.S., L.H., K.W., S.K., C.M.F.; Writing - original draft: M. Bachmann, M.S.; Writing - review & editing: M. Bachmann, M.S., V.V.M., C.M.F., V.P.H., B.W.-H., M. Bastmeyer; Visualization: M. Bachmann, M.S., V.V.M.; Supervision: M. Bachmann, M.S., V.P.H., B.W.-H., M. Bastmeyer; Project administration: M. Bachmann, B.W.-H., M. Bastmeyer; Funding acquisition: B.W.-H., M. Bastmeyer.

**Funding**
This work was supported by Deutsche Forschungsgemeinschaft [BA 6471/1-1 and Karlsruhe School of Optics and Photonics PhD scholarship to M. Bachmann], Baden-Württemberg Stiftung [state scholarship to M.S.], the Academy of Finland [290506 to V.P.H.] and Opetushallitus [postdoctoral fellowship to V.V.M.]. Schweizerischer Nationalfonds zur Förderung der Wissenschaftlichen Forschung supported the work of M. Bachmann, M.R., and B.W.-H. [31003A_166384 and 310030L_170112/1].

**Supplementary information**
Supplementary information available online at
http://jcs.biologists.org/lookup/doi/10.1242/jcs.242404.supplemental

**Peer review history**
The peer review history is available online at
https://jcs.biologists.org/lookup/doi/10.1242/jcs.242404.reviewer-comments.pdf

**References**

**Attieh, Y., Clark, A. G., Grass, C., Richon, S., Pocard, M., Mariani, P., Elkhatib, N., Betz, T., Gurchenkov, B. and Vignjevic, D. M.** (2017). Cancer-associated fibroblasts lead tumor invasion through integrin-beta3-dependent fibronectin assembly. *J Cell Biol*. **216**, 3509-3520. doi:10.1083/jcb.201702033

**Bachmann, M., Kukkurainen, S., Hytönen, V. P. and Wehrle-Haller, B.** (2019). Cell adhesion by integrins. *Physiol. Rev.* **99**, 1655-1699. doi:10.1152/physrev.00036.2018

**Ballestrem, C., Hinz, B., Imhof, B. A. and Wehrle-Haller, B.** (2001). Marching at the front and dragging behind: differential alphaVbeta3-integrin turnover regulates focal adhesion behavior. *J. Cell Biol.* **155**, 1319-1332. doi:10.1083/jcb.200107107

**Benito-Jardón, M., Klapproth, S., Gimeno-LLuch, I., Petzold, T., Bharadwaj, M., Müller, D. J., Zuchtriegel, G., Reichel, C. A and Costell, M.** (2017). The fibronectin synergy site re-enforces cell adhesion and mediates a crosstalk between integrin classes. *eLife* **6**, e22264. doi:10.7554/eLife.22264

**Berendsen, H. J. C., Postma, J. P. M., van Gunsteren, W. F., DiNola, A. and Haak, J. R.** (1984). Molecular dynamics with coupling to an external bath. *J. Chem. Phys.* **81**, 3684-3690. doi:10.1063/1.448118

**Bolte, S. and Cordelieres, F. P.** (2006). A guided tour into subcellular colocalization analysis in light microscopy. *J. Microsc.* **224**, 213-232. doi:10.1111/j.1365-2818.2006.01706.x

**Brunner, M., Millon-Frémillon, A., Chevalier, G., Nakchbandi, I. A., Mosher, D., Block, M. R., Albigès-Rizo, C. and Bouvard, D.** (2011). Osteoblast mineralization requires beta1 integrin/ICAP-1-dependent fibronectin deposition. *J. Cell Biol.* **194**, 307-322. doi:10.1083/jcb.201007108

**Bussi, G., Donadio, D. and Parrinello, M.** (2007). Canonical sampling through velocity rescaling. *J. Chem. Phys.* **126**, 014101. doi:10.1063/1.2408420

**Byron, A., Humphries, J. D., Bass, M. D., Knight, D. and Humphries, M. J.** (2011). Proteomic analysis of integrin adhesion complexes. *Sci. Signal.* **4**, pt2. doi:10.1126/scisignal.2002165

**Campbell, I. D. and Humphries, M. J.** (2011). Integrin structure, activation, and interactions. *Cold Spring Harb. Perspect. Biol.* **3**, a004994. doi:10.1101/cshperspect.a004994

**Chen, Y., Ju, L. A., Zhou, F., Liao, J., Xue, L., Su, Q. P., Jin, D., Yuan, Y., Lu, H., Jackson, S. P. et al.** (2019). An integrin $\alpha\alpha$IIb$\beta$3 intermediate affinity state mediates biomechanical platelet aggregation. *Nat. Mater.* **18**, 760-769. doi:10.1038/s41563-019-0323-6

**Chillakuri, C. R., Jones, C. and Mardon, H. J.** (2010). Heparin binding domain in vitronectin is required for oligomerization and thus enhances integrin mediated cell adhesion and spreading. *FEBS Lett.* **584**, 3287-3291. doi:10.1016/j.febslet.2010.06.023

**Cluzel, C., Saltel, F., Lussi, J., Paulhe, F., Imhof, B. A. and Wehrle-Haller, B.** (2005). The mechanisms and dynamics of alphavbeta3 integrin clustering in living cells. *J. Cell Biol.* **171**, 383-392. doi:10.1083/jcb.200503017

**Cormier, A., Campbell, M. G., Ito, S., Wu, S., Lou, J., Marks, J., Baron, J. L., Nishimura, S. L. and Cheng, Y.** (2018). Cryo-EM structure of the alphavbeta8 integrin reveals a mechanism for stabilizing integrin extension. *Nat. Struct. Mol. Biol.* **25**, 698-704. doi:10.1038/s41594-018-0093-x

**Dai, A., Ye, F., Taylor, D. W., Hu, G., Ginsberg, M. H. and Taylor, K. A.** (2015). The structure of a full-length membrane-embedded integrin bound to a physiological ligand. *J. Biol. Chem.* **290**, 27168-27175. doi:10.1074/jbc.M115.682377

**Danen, E. H., Sonneveld, P., Brakebusch, C., Fassler, R. and Sonnenberg, A.** (2002). The fibronectin-binding integrins alpha5beta1 and alphavbeta3 differentially modulate RhoA-GTP loading, organization of cell matrix adhesions, and fibronectin fibrillogenesis. *J. Cell Biol.* **159**, 1071-1086. doi:10.1083/jcb.200205014

**Dao, L., Weiland, U., Hauser, M., Nazarenko, I., Kalt, H., Bastmeyer, M. and Franz, C. M.** (2012). Revealing non-genetic adhesive variations in clonal populations by comparative single-cell force spectroscopy. *Exp. Cell Res.* **318**, 2155-2167. doi:10.1016/j.yexcr.2012.06.017

**Elosegui-Artola, A., Oria, R., Chen, Y., Kosmalska, A., Pérez-González, C., Castro, N., Zhu, C., Trepat, X and Roca-Cusachs, P.** (2016). Mechanical regulation of a molecular clutch defines force transmission and transduction in response to matrix rigidity. *Nat. Cell Biol.* **18**, 540-548. doi:10.1038/ncb3336

**Eng, E. T., Smagghe, B. J., Walz, T. and Springer, T. A.** (2011). Intact alpha$_{IIb}$beta3 integrin is extended after activation as measured by solution X-ray scattering and electron microscopy. *J. Biol. Chem.* **286**, 35218-35226. doi:10.1074/jbc.M111.275107

**Engler, A. J., Chan, M., Boettiger, D. and Schwarzbauer, J. E.** (2009). A novel mode of cell detachment from fibrillar fibronectin matrix under shear. *J. Cell Sci.* **122**, 1647-1653. doi:10.1242/jcs.040824

**Erdogan, B., Ao, M., White, L. M., Means, A. L., Brewer, B. M., Yang, L., Washington, M. K., Shi, C., Franco, O. E., Weaver, A. M. et al.** (2017). Cancer-associated fibroblasts promote directional cancer cell migration by aligning fibronectin. *J. Cell Biol.* **216**, 3799-3816. doi:10.1083/jcb.201704053

**Fan, Z., McArdle, S., Marki, A., Mikulski, Z., Gutierrez, E., Engelhardt, B., Deutsch, U., Ginsberg, M., Groisman, A. and Ley, K.** (2016). Neutrophil recruitment limited by high-affinity bent $\beta$2 integrin binding ligand in cis. *Nat. Commun.* **7**, 12658. doi:10.1038/ncomms12658

**Fan, Z., Kiosses, W. B., Sun, H., Orecchioni, M., Ghosheh, Y., Zajonc, D. M., Arnaout, M. A., Gutierrez, E., Groisman, A., Ginsberg, M. H. et al.** (2019). High-affinity bent $\beta_2$-integrin molecules in arresting neutrophils face each other through binding to ICAMs in cis. *Cell Rep.* **26**, 119-130.e5. doi:10.1016/j.celrep.2018.12.038

**Fernandez-Sauze, S., Grall, D., Cseh, B. and Van Obberghen-Schilling, E.** (2009). Regulation of fibronectin matrix assembly and capillary morphogenesis in endothelial cells by Rho family GTPases. *Exp. Cell Res.* **315**, 2092-2104. doi:10.1016/j.yexcr.2009.03.017

**Fiore, V. F., Strane, P. W., Bryksin, A. V., White, E. S., Hagood, J. S. and Barker, T. H.** (2015). Conformational coupling of integrin and Thy-1 regulates Fyn priming and fibroblast mechanotransduction. *J. Cell Biol.* **211**, 173-190. doi:10.1083/jcb.201505007

**Franco-Barraza, J., Beacham, D. A., Amatangelo, M. D. and Cukierman, E.** (2016). Preparation of extracellular matrices produced by cultured and primary fibroblasts. *Curr. Protoc. Cell Biol.* **71**, 10.19.1-10.19.34. doi:10.1002/cpcb.2

**Geissinger, E., Weisser, C., Fischer, P., Schartl, M. and Wellbrock, C.** (2002). Autocrine stimulation by osteopontin contributes to antiapoptotic signalling of melanocytes in dermal collagen. *Cancer Res.* **62**, 4820-4828.

**George, E. L., Georges-Labouesse, E. N., Patel-King, R. S., Rayburn, H. and Hynes, R. O.** (1993). Defects in mesoderm, neural tube and vascular development in mouse embryos lacking fibronectin. *Development* **119**, 1079-1091.

**Gladson, C. L., Wilcox, J. N., Sanders, L., Gillespie, G. Y. and Cheresh, D. A.** (1995). Cerebral microenvironment influences expression of the vitronectin gene in astrocytic tumors. *J. Cell Sci.* **108**, 947-956.

**Gudzenko, T. and Franz, C. M.** (2015). Studying early stages of fibronectin fibrillogenesis in living cells by atomic force microscopy. *Mol. Biol. Cell* **26**, 3190-3204. doi:10.1091/mbc.e14-05-1026

**Hodivala-Dilke, K. M., McHugh, K. P., Tsakiris, D. A., Rayburn, H., Crowley, D., Ullman-Culleré, M., Ross, F. P., Coller, B. S., Teitelbaum, S. and Hynes, R. O.** (1999). Beta3-integrin-deficient mice are a model for Glanzmann thrombasthenia showing placental defects and reduced survival. *J. Clin. Invest.* **103**, 229-238. doi:10.1172/JCI5487

**Humphries, J. D., Byron, A. and Humphries, M. J.** (2006). Integrin ligands at a glance. *J. Cell Sci.* **119**, 3901-3903. doi:10.1242/jcs.03098

**Humphries, J. D., Wang, P., Streuli, C., Geiger, B., Humphries, M. J. and Ballestrem, C.** (2007). Vinculin controls focal adhesion formation by direct interactions with talin and actin. *J. Cell Biol.* **179**, 1043-1057. doi:10.1083/jcb.200703036

**Hytönen, V. P. and Wehrle-Haller, B.** (2014). Protein conformation as a regulator of cell-matrix adhesion. *Phys. Chem. Chem. Phys.* **16**, 6342-6357. doi:10.1039/C3CP54884H

**Jorgensen, W. L. and Madura, J. D.** (1983). Quantum and statistical mechanical studies of liquids. 25. Solvation and conformation of methanol in water. *J. Am. Chem. Soc.* **105**, 1407-1413. doi:10.1021/ja00344a001

**Kandow, C. E., Georges, P. C., Janmey, P. A. and Beningo, K. A.** (2007). Polyacrylamide hydrogels for cell mechanics: steps toward optimization and alternative uses. *Methods Cell Biol.* **83**, 29-46. doi:10.1016/S0091-679X(07)83002-0

**Kaukonen, R., Jacquemet, G., Hamidi, H. and Ivaska, J.** (2017). Cell-derived matrices for studying cell proliferation and directional migration in a complex 3D microenvironment. *Nat. Protoc.* **12**, 2376-2390. doi:10.1038/nprot.2017.107

**Keasey, M. P., Jia, C., Pimentel, L. F., Sante, R. R., Lovins, C. and Hagg, T.** (2018). Blood vitronectin is a major activator of LIF and IL-6 in the brain through integrin-FAK and uPAR signaling. *J. Cell Sci.* **131**, jcs202580. doi:10.1242/jcs.202580

**Kronenberg, N. M., Liehm, P., Steude, A., Knipper, J. A., Borger, J. G., Scarcelli, G., Franze, K., Powis, S. J. and Gather, M. C.** (2017). Long-term imaging of cellular forces with high precision by elastic resonator interference stress microscopy. *Nat. Cell Biol.* **19**, 864-872. doi:10.1038/ncb3561

**Kuo, J.-C., Han, X., Hsiao, C. T., Yates, J. R., III and Waterman, C. M.** (2011). Analysis of the myosin-II-responsive focal adhesion proteome reveals a role for beta-Pix in negative regulation of focal adhesion maturation. *Nat. Cell Biol.* **13**, 383-393. doi:10.1038/ncb2216

**Langhe, R. P., Gudzenko, T., Bachmann, M., Becker, S. F., Gonnermann, C., Winter, C., Abbruzzese, G., Alfandari, D., Kratzer, M.-C., Franz, C. M. et al.** (2016). Cadherin-11 localizes to focal adhesions and promotes cell-substrate adhesion. *Nat. Commun.* **7**, 10909. doi:10.1038/ncomms10909

**Lehnert, D., Wehrle-Haller, B., David, C., Weiland, U., Ballestrem, C., Imhof, B. A. and Bastmeyer, M.** (2004). Cell behaviour on micropatterned substrata: limits of extracellular matrix geometry for spreading and adhesion. *J. Cell Sci.* **117**, 41-52. doi:10.1242/jcs.00836

**Li, J., Su, Y., Xia, W., Qin, Y., Humphries, M. J., Vestweber, D., Cabañas, C., Lu, C. and Springer, T. A.** (2017). Conformational equilibria and intrinsic affinities define integrin activation. *EMBO J.* **36**, 629-645. doi:10.15252/embj.201695803

**Lindorff-Larsen, K., Piana, S., Palmo, K., Maragakis, P., Klepeis, J. L., Dror, R. O. and Shaw, D. E.** (2010). Improved side-chain torsion potentials for the Amber ff99SB protein force field. *Proteins* **78**, 1950-1958. doi:10.1002/prot.22711

**Luo, B. H., Springer, T. A. and Takagi, J.** (2003). Stabilizing the open conformation of the integrin headpiece with a glycan wedge increases affinity for ligand. *Proc. Natl. Acad. Sci. USA* **100**, 2403-2408. doi:10.1073/pnas.0438060100

**Mas-Moruno, C., Rechenmacher, F. and Kessler, H**. (2010). Cilengitide: the first anti-angiogenic small molecule drug candidate design, synthesis and clinical evaluation. *Anticancer Agents Med. Chem.* **10**, 753-768. doi:10.2174/187152010794728639

**Mierke, C. T., Kollmannsberger, P., Zitterbart, D. P., Diez, G., Koch, T. M., Marg, S., Ziegler, W. H., Goldmann, W. H. and Fabry, B.** (2010). Vinculin facilitates cell invasion into three-dimensional collagen matrices. *J. Biol. Chem.* **285**, 13121-13130. doi:10.1074/jbc.M109.087171

**Miyazaki, N., Iwasaki, K. and Takagi, J.** (2018). A systematic survey of conformational states in beta1 and beta4 integrins using negative-stain electron microscopy. *J. Cell Sci.* **131**, jcs216754. doi:10.1242/jcs.216754

**Orlando, R. A. and Cheresh, D. A.** (1991). Arginine-glycine-aspartic acid binding leading to molecular stabilization between integrin alpha v beta 3 and its ligand. *J. Biol. Chem.* **266**, 19543-19550.

**Pankov, R. and Yamada, K. M.** (2002). Fibronectin at a glance. *J. Cell Sci.* **115**, 3861-3863. doi:10.1242/jcs.00059

**Pierschbacher, M. D. and Ruoslahti, E.** (1987). Influence of stereochemistry of the sequence Arg-Gly-Asp-Xaa on binding specificity in cell adhesion. *J. Biol. Chem.* **262**, 17294-17298.

**Pinon, P., Pärssinen, J., Vazquez, P., Bachmann, M., Rahikainen, R., Jacquier, M.-C., Azizi, L., Määttä, J. A., Bastmeyer, M., Hytönen, V. P. et al.** (2014). Talin-bound NPLY motif recruits integrin-signaling adapters to regulate cell spreading and mechanosensing. *J. Cell Biol.* **205**, 265-281. doi:10.1083/jcb.201308136

**Plotnikov, S. V., Sabass, B., Schwarz, U. S. and Waterman, C. M.** (2014). High-resolution traction force microscopy. *Methods Cell Biol.* **123**, 367-394. doi:10.1016/B978-0-12-420138-5.00020-3

**Preissner, K. T. and Reuning, U.** (2011). Vitronectin in vascular context: facets of a multitalented matricellular protein. *Semin. Thromb. Hemost.* **37**, 408-424. doi:10.1055/s-0031-1276590

**Puklin-Faucher, E., Gao, M., Schulten, K. and Vogel, V.** (2006). How the headpiece hinge angle is opened: new insights into the dynamics of integrin activation. *J. Cell Biol.* **175**, 349-360. doi:10.1083/jcb.200602071

**Pytela, R., Pierschbacher, M. D. and Ruoslahti, E.** (1985). A 125/115-kDa cell surface receptor specific for vitronectin interacts with the arginine-glycine-aspartic acid adhesion sequence derived from fibronectin. *Proc. Natl. Acad. Sci. USA* **82**, 5766-5770. doi:10.1073/pnas.82.17.5766

**Rahikainen, R., von Essen, M., Schaefer, M., Qi, L., Azizi, L., Kelly, C., Ihalainen, T. O., Wehrle-Haller, B., Bastmeyer, M., Huang, C. et al.** (2017). Mechanical stability of talin rod controls cell migration and substrate sensing. *Sci. Rep.* **7**, 3571. doi:10.1038/s41598-017-03335-2

**Richter, B., Hahn, V., Bertels, S., Claus, T. K., Wegener, M., Delaittre, G., Barner-Kowollik, C. and Bastmeyer, M.** (2017). Guiding cell attachment in 3D microscaffolds selectively functionalized with two distinct adhesion proteins. *Adv. Mater.* **29**, 1604342. doi:10.1002/adma.201604342

**Roca-Cusachs, P., Gauthier, N. C., Del Rio, A. and Sheetz, M. P.** (2009). Clustering of alpha(5)beta(1) integrins determines adhesion strength whereas alpha(v)beta(3) and talin enable mechanotransduction. *Proc. Natl. Acad. Sci. USA* **106**, 16245-16250. doi:10.1073/pnas.0902818106

**Saltel, F., Mortier, E., Hytönen, V. P., Jacquier, M.-C., Zimmermann, P., Vogel, V., Liu, W. and Wehrle-Haller, B.** (2009). New PI(4,5)P2- and membrane proximal integrin-binding motifs in the talin head control beta3-integrin clustering. *J. Cell Biol.* **187**, 715-731. doi:10.1083/jcb.200908134

**Schiller, H. B., Friedel, C. C., Boulegue, C. and Fässler, R.** (2011). Quantitative proteomics of the integrin adhesome show a myosin II-dependent recruitment of LIM domain proteins. *EMBO Rep.* **12**, 259-266. doi:10.1038/embor.2011.5

**Schiller, H. B., Hermann, M. R., Polleux, J., Vignaud, T., Zanivan, S., Friedel, C. C., Sun, Z., Raducanu, A., Gottschalk, K.-E., Théry, M. et al.** (2013). β1- and αv-class integrins cooperate to regulate myosin II during rigidity sensing of fibronectin-based microenvironments. *Nat. Cell Biol.* **15**, 625-636. doi:10.1038/ncb2747

**Schindelin, J., Rueden, C. T., Hiner, M. C. and Eliceiri, K. W**. (2015). The ImageJ ecosystem: an open platform for biomedical image analysis. *Mol. Reprod. Dev.* **82**, 518-529. doi:10.1002/mrd.22489

**Soto-Ribeiro, M., Kastberger, B., Bachmann, M., Azizi, L., Fouad, K., Jacquier, M.-C., Boettiger, D., Bouvard, D., Bastmeyer, M., Hytönen, V. P. et al.** (2019). β1D integrin splice variant stabilizes integrin dynamics and reduces integrin signaling by limiting paxillin recruitment. *J. Cell Sci.* **132**, jcs224493. doi:10.1242/jcs.224493

**Sousa da Silva, A. W. and Vranken, W. F.** (2012). ACPYPE - antechamber python parser interface. *BMC Res. Notes* **5**, 367. doi:10.1186/1756-0500-5-367

**Takagi, J., Petre, B. M., Walz, T. and Springer, T. A.** (2002). Global conformational rearrangements in integrin extracellular domains in outside-in and inside-out signaling. *Cell* **110**, 599-611. doi:10.1016/S0092-8674(02)00935-2

**Takahashi, S., Leiss, M., Moser, M., Ohashi, T., Kitao, T., Heckmann, D., Pfeifer, A., Kessler, H., Takagi, J., Erickson, H. P. et al.** (2007). The RGD motif in fibronectin is essential for development but dispensable for fibril assembly. *J. Cell Biol.* **178**, 167-178. doi:10.1083/jcb.200703021

**Thievessen, I., Thompson, P. M., Berlemont, S., Plevock, K. M., Plotnikov, S. V., Zemljic-Harpf, A., Ross, R. S., Davidson, M. W., Danuser, G., Campbell, S. L. et al.** (2013). Vinculin-actin interaction couples actin retrograde flow to focal adhesions, but is dispensable for focal adhesion growth. *J. Cell Biol.* **202**, 163-177. doi:10.1083/jcb.201303129

**van der Flier, A., Badu-Nkansah, K., Whittaker, C. A., Crowley, D., Bronson, R. T., Lacy-Hulbert, A. and Hynes, R. O.** (2010). Endothelial alpha5 and alphav integrins cooperate in remodeling of the vasculature during development. *Development* **137**, 2439-2449. doi:10.1242/dev.049551

**Van Der Spoel, D., Lindahl, E., Hess, B., Groenhof, G., Mark, A. E. and Berendsen, H. J.** (2005). GROMACS: fast, flexible, and free. *J. Comput. Chem.* **26**, 1701-1718. doi:10.1002/jcc.20291

**Wang, S., Wu, C., Zhang, Y., Zhong, Q., Sun, H., Cao, W., Ge, G., Li, G., Zhang, X. F and Chen, J.** (2018). Integrin alpha4beta7 switches its ligand specificity via distinct conformer-specific activation. *J. Cell Biol.* **217**, 2799-2812. doi:10.1083/jcb.201710022

**Wehrle-Haller, B.** (2007). Analysis of integrin dynamics by fluorescence recovery after photobleaching. *Methods Mol. Biol.* **370**, 173-201. doi:10.1007/978-1-59745-353-0_13

**Wennerberg, K., Lohikangas, L., Gullberg, D., Pfaff, M., Johansson, S. and Fassler, R.** (1996). Beta 1 integrin-dependent and -independent polymerization of fibronectin. *J. Cell Biol.* **132**, 227-238. doi:10.1083/jcb.132.1.227

**White, D. P., Caswell, P. T. and Norman, J. C.** (2007). alphavbeta3 and alpha5beta1 integrin recycling pathways dictate downstream Rho kinase signaling to regulate persistent cell migration. *J. Cell Biol.* **177**, 515-525. doi:10.1083/jcb.200609004

**Xiong, J. P., Stehle, T., Zhang, R., Joachimiak, A., Frech, M., Goodman, S. L. and Arnaout, M. A.** (2002). Crystal structure of the extracellular segment of integrin alpha Vbeta3 in complex with an Arg-Gly-Asp ligand. *Science* **296**, 151-155. doi:10.1126/science.1069040

**Yang, J. T., Bader, B. L., Kreidberg, J. A., Ullman-Culleré, M., Trevithick, J. E. and Hynes, R. O.** (1999). Overlapping and independent functions of fibronectin

receptor integrins in early mesodermal development. *Dev. Biol.* **215**, 264-277. doi:10.1006/dbio.1999.9451

**Ye, F., Hu, G., Taylor, D., Ratnikov, B., Bobkov, A. A., McLean, M. A., Sligar, S. G., Taylor, K. A. and Ginsberg, M. H.** (2010). Recreation of the terminal events in physiological integrin activation. *J. Cell Biol.* **188**, 157-173. doi:10.1083/jcb.200908045

**Zhu, J., Luo, B. H., Xiao, T., Zhang, C., Nishida, N. and Springer, T. A.** (2008). Structure of a complete integrin ectodomain in a physiologic resting state and activation and deactivation by applied forces. *Mol. Cell* **32**, 849-861. doi:10.1016/j.molcel.2008.11.018

**Zhu, J. and Springer, T. A.** (2013). Complete integrin headpiece opening in eight steps. *J. Cell Biol.* **201**, 1053-1068. doi:10.1083/jcb.201212037